Monthly Notices
of the
ROYAL ASTRONOMICAL SOCIETY

Mon. Not. R. Astron. Soc. **426,** 3225–3240 (2012) doi:10.1111/j.1365-2966.2012.21959.x

Simultaneous X-ray and optical observations of true type 2 Seyfert galaxies⋆

Stefano Bianchi,[1]† Francesca Panessa,[2] Xavier Barcons,[3] Francisco J. Carrera,[3] Fabio La Franca,[1] Giorgio Matt,[1] Francesca Onori,[1] Anna Wolter,[4] Amalia Corral,[5] Lorenzo Monaco,[6] Ángel Ruiz[3,7] and Murray Brightman[8]

[1]*Dipartimento di Fisica, Università degli Studi Roma Tre, via della Vasca Navale 84, 00146 Roma, Italy*
[2]*Istituto di Astrofisica Spaziale e Fisica Cosmica (IASF-INAF), via del Fosso del Cavaliere 100, 00133 Roma, Italy*
[3]*Instituto de Física de Cantabria (CSIC-Universidad de Cantabria), 39005 Santander, Spain*
[4]*INAF-Osservatorio Astronomico di Brera, via Brera 28, 20121, Milano, Italy*
[5]*Institute of Astronomy & Astrophysics, National Observatory of Athens, Palaia Penteli 15236, Athens, Greece*
[6]*European Southern Observatory, 19001 Casilla, Santiago, Chile*
[7]*Inter-University Centre for Astronomy and Astrophysics (IUCAA), Post Bag 4, Ganeshkhind, Pune 411 007, India*
[8]*Max-Planck-Institut für Extraterrestrische Physik, Giessenbachstrasse 1, D-85748, Garching bei Mnchen, Germany*

Accepted 2012 August 20. Received 2012 August 16; in original form 2012 June 22

ABSTRACT

We present the results of a campaign of simultaneous X-ray and optical observations of 'true' type 2 Seyfert galaxies candidates, i.e. active galactic nuclei without a broad-line region (BLR). Out of the initial sample composed of eight sources, one object, IC 1631, was found to be a misclassified starburst galaxy, another, Q2130−431, does show broad optical lines, while other two, IRAS 01428−0404 and NGC 4698, are very likely absorbed by Compton-thick gas along the line of sight. Therefore, these four sources are not unabsorbed Seyfert 2s as previously suggested in the literature. On the other hand, we confirm that NGC 3147, NGC 3660 and Q2131−427 belong to the class of true type 2 Seyfert galaxies, since they do not show any evidence for a broad component of the optical lines nor for obscuration in their X-ray spectra. These three sources have low accretion rates ($\dot{m} = L_{\rm bol}/L_{\rm Edd} \lesssim 0.01$), in agreement with theoretical models which predict that the BLR disappears below a critical value of $L_{\rm bol}/L_{\rm Edd}$. The last source, Mrk 273x, would represent an exception even of these accretion-dependent versions of the Unification Models, due to its high X-ray luminosity and accretion rate, and no evidence for obscuration. However, its optical classification as a Seyfert 2 is only based on the absence of a broad component of Hβ, due to the lack of optical spectra encompassing the Hα band.

Key words: galaxies: active – galaxies: Seyfert.

1 INTRODUCTION

The fundamental idea behind the standard Unified Model (Antonucci 1993) is that type 1 and type 2 active galactic nuclei (AGN) have no intrinsic physical differences, their classification being instead determined by the presence or absence of absorbing material along the line of sight to the object. This scenario has been extremely successful, although some additional ingredients are needed in order to take into account all the observational evidence (see Bianchi, Maiolino & Risaliti 2012 for a review). Among the failed expectations of the Unification Model is the lack of broad optical lines in the polarized spectra of about half of the brightest Seyfert 2 (Sy2) galaxies, even when high-quality spectropolarimetric data are available (e.g. Tran 2001, 2003).

⋆Based on observations obtained with *XMM–Newton*, an ESA science mission with instruments and contributions directly funded by ESA Member States and the USA (NASA); with the TNG and Nordic Optical Telescope (NOT) operated on the island of La Palma by the Centro Galileo Galilei and the Nordic Optical Telescope Science Association, respectively, in the Spanish Observatorio del Roque de los Muchachos; at the Centro Astronómico Hispano Alemán (CAHA) at Calar Alto, operated jointly by the Max-Planck-Institut für Astronomie and the Instituto de Astrofísica de Andalucía (CSIC); at the European Organisation for Astronomical Research in the Southern hemisphere, Chile: 278.B-5021(A), 278.B-5016(A); at the Observatorio de Sierra Nevada (OSN) operated by the Instituto de Astrofísica de Andalucía (CSIC).

†E-mail: bianchi@fis.uniroma3.it

These Sy2 galaxies without a hidden broad line region (BLR) are observationally found to accrete at low Eddington rates (e.g. Nicastro, Martocchia & Matt 2003; Bian & Gu 2007; Shu et al. 2007; Wu et al. 2011; Marinucci et al. 2012). This is in agreement with theoretical models which predict that the BLR disappears below a certain critical value of accretion rate and/or luminosity (e.g. Nicastro 2000; Elitzur & Ho 2009; Trump et al. 2011). If the BLR cannot form in weakly accreting AGN, we expect the existence of the unobscured counterparts of the non-hidden BLR Sy2 galaxies, that is, optically classified type 2 objects, without any evidence of obscuration in their X-ray spectrum. In the last 10 yr, a significant number of such 'true' type 2 Seyfert galaxies have been claimed in the literature (e.g. Pappa et al. 2001; Panessa & Bassani 2002; Boller et al. 2003; Wolter et al. 2005; Gliozzi, Sambruna & Foschini 2007; Bianchi et al. 2008; Brightman & Nandra 2008; Panessa et al. 2009; Shi et al. 2010; Tran, Lyke & Mader 2011; Trump et al. 2011), with one case in which the BLR is present but characterized by an intrinsically high Balmer decrement (Corral et al. 2005). Most of these sources have the low accretion rates/luminosities required by the above-mentioned theoretical models.

Nevertheless, a homogeneous and unambiguous sample of true type 2 Seyfert galaxies is still missing. One of the main issues is that sources may be highly variable and may change their optical and/or X-ray appearance in different observations. These changing-look AGN are not uncommon. In some cases, this behaviour is best explained by a real 'switching-off' of the nucleus (see e.g. Gilli et al. 2000; Guainazzi et al. 2005a), but a variable column density of the absorber appears as the best explanation in the majority of the cases (e.g. Elvis et al. 2004; Risaliti et al. 2005; Bianchi et al. 2009b; Bianchi et al. 2012, and references therein). If the optical and the X-ray spectrum are taken in two different states of the source, then it is clear that the disagreement between the two classifications may be only apparent. Therefore, the key to find genuine unabsorbed Sy2s is to perform simultaneous X-ray and optical observations. Only two unabsorbed Sy2 candidates have been observed so far simultaneously in the X-rays and the optical band, leading to the discovery of two unambiguous true type Sy2s: NGC 3147 (Bianchi et al. 2008) and Q2131−427 (Panessa et al. 2009). In this paper, we report on the results of the complete systematic campaign of simultaneous X-ray and optical observations of eight true type 2 Seyfert galaxies candidates.

2 THE SAMPLE

In order to build a comprehensive sample of unabsorbed Sy2 candidates, we started from the Panessa & Bassani (2002) sample, which includes 17 type 2 Seyfert galaxies with an X-ray column density less than 10^{22} cm^{-2} and very unlikely to be Compton thick, as suggested by isotropic indicators. We selected a conservative subsample, excluding the sources where an intrinsic column density (even if much lower than the one expected from the optical properties) is actually measured. Therefore, we only chose sources which are genuinely unabsorbed, in the sense that no column density in excess of the Galactic one has ever been observed in the X-rays, with tight upper limits (at most few 10^{21} cm^{-2}; Panessa & Bassani 2002). Moreover, three other sources (NGC 4565, NGC 4579 and IRAS 20051−1117) were excluded because they were found to be misclassified in the optical, all having broad components of the emission lines (Ho et al. 1997b; Georgantopoulos et al. 2004). Another one (NGC 7590) was found to be a Compton-thick Sy2 dominated by a nearby off-nuclear ultraluminous X-ray source (ULX; Shu, Liu & Wang 2010), while NGC 7679 is dominated by starburst emission in the optical band (della Ceca et al. 2001).

To the remaining five objects, we added two sources belonging to a sample of 'naked' AGN, i.e. spectroscopically classified as Sy2s, but with very large amplitude variations in the B_J passband, typical of type 1 objects, where the nucleus is directly seen without intervening absorption (Hawkins 2004). The sources included in our sample were selected from the three objects with *Chandra* data presented by Gliozzi et al. (2007), supporting their unabsorbed nature, excluding Q2122−444, which, re-observed simultaneously with *XMM–Newton* and New Technology Telescope (NTT), revealed the presence of broad optical line components, thus ruling out the true type 2 hypothesis (Gliozzi et al. 2010). Finally, we added to our sample NGC 3660 a very promising unabsorbed Sy2 candidate suggested by Brightman & Nandra (2008).

The final sample (Table 1) consists of eight sources, which we observed with *XMM–Newton*. As mentioned in Section 1, to avoid any possible misclassification due to variability of the sources, we coordinated all the *XMM–Newton* observations with quasi-simultaneous ground-based optical spectroscopy. As a final note, we would like to stress that, given the heterogeneous selection methods described above, this sample is by no means complete in any sense.

3 OBSERVATIONS AND DATA REDUCTION

3.1 *XMM–Newton*

The *XMM–Newton* observations of the sources of our sample are listed in Table 1. In all cases, the observations were performed with the European Photon Imaging Camera (EPIC) CCD cameras, the pn and the two MOS, operated in Large and Small Window, respectively, and Medium Filter. Data were reduced with SAS 8.0.0 and the screening for intervals of flaring particle background was done consistently with the choice of extraction radii, in an iterative process based on the procedure to maximize the signal-to-noise ratio described in detail by Piconcelli et al. (2004) in their appendix A. The background spectra were extracted from source-free circular regions with a radius of 50 arcsec. The MOS data have only been used when the number of counts in their spectra was high enough to significantly help in the analysis. Finally, spectra were binned in order to oversample the instrumental resolution by at least a factor of 3 and to have no less than 20 counts in each background-subtracted spectral channel. The latter requirement allows us to use the χ^2 statistics. When the number of counts was too low (as in the cases of IRAS 01428−0404 and NGC 4698), we performed a binning with less counts per bin and adopted the Cash (1976) statistics. Similarly, in order to look for the iron Kα emission lines in low-count spectra, we also performed local fits with the unbinned spectra (in a restricted energy band of 350 channels centred around the rest frame 6.4 keV) with the Cash statistics (see e.g. Guainazzi, Matt & Perola 2005b; Bianchi, Guainazzi & Chiaberge 2006).

In the following, errors and upper limits correspond to the 90 per cent confidence level for one interesting parameter ($\Delta\chi^2 = 2.71$), unless otherwise stated. The adopted cosmological parameters are $H_0 = 70\,\mathrm{km\,s^{-1}\,Mpc^{-1}}$, $\Omega_\Lambda = 0.73$ and $\Omega_\mathrm{m} = 0.27$ (i.e. the default ones in XSPEC 12.7.1; Arnaud 1996).

3.2 Optical data

Optical spectroscopy of our 'true' Sy2 candidates was obtained with a variety of ground-based telescopes and instruments, as detailed

Table 1. The sample of true type Sy2 candidates analysed in this paper, along with the details of the quasi-simultaneous X-ray and optical/NIR observations.

Name	z	*XMM–Newton*			Optical/NIR					
		Obs. date	Obs. ID	Exp.	Obs. date	Instr.	Slit (arcsec)	Exp.	Range	$\lambda/\Delta\lambda$
IC 1631	0.030 968	2006-11-23	0405020801	22	2006-12-01	VLT/FORS2/300V	1.0	1200	4450–8700	440
IRAS 01428−0404	0.018 199	2008-08-03	0550940201	18	2008-07-30	CAHA/CAFOS/G-100	1.8	1800 × 2	4900–7800	880
Mrk 273x	0.458 000	2010-05-13	0651360301	14	2010-05-17	TNG/LRS/LR-R	1.0	1800	4470–10 073	714
		2010-05-15	0651360501	15						
		2010-05-17	0651360601	14						
		2010-06-26	0651360701	11						
NGC 3147	0.009 346	2006-10-06	0405020601	17	2006-10-04	OSN/Albireo	2.0	1800×6	4000–7000	1500
					2006-10-05					
					2006-10-09					
NGC 3660	0.012 285	2009-06-03	0601560201	15	2010-01-15	NOT/ALFOSC/Gr7	0.5	300 × 2	3850–6850	1300
					2011-02-04	TNG/LRS/LR-B	0.7	120	3000–8430	835
					2011-02-04	TNG/LRS/LR-R	0.7	60	4470–10 073	1020
					2011-00-00	TNG/NICS/IJ	0.75	360 × 4	9000–14 500	665
					2011-00-00	TNG/NICS/JS	0.75	945 × 4	11700–13 300	1600
NGC 4698	0.003 366	2010-06-09	0651360401	33	2010-12-28	NOT/ALFOSC/Gr7	0.5	30 × 2	3850–6850	1300
Q2130−431	0.266	2006-11-13	0402460201	32	2006-12-20	NTT/EMMI/Gr4	1.0	1200	5500–10 000	613
Q2131−427	0.365	2006-11-15	0402460401	27	2006-12-20	NTT/EMMI/Gr4	1.0	1200	5500–10 000	613

Notes. Col. (1) Source. (2) Redshift (NED). (3–5) *XMM–Newton* observation date, observation ID and exposure time (ks). (6–11) Optical/NIR observation date, instruments, adopted slit, exposures (s), wavelength range (Å) and resolution.

in Table 1. All the optical observations took place within a few days up to few months of the *XMM–Newton* X-ray observations. For the purposes of our study, these observations can be considered 'simultaneous', since we expect the optical spectroscopy and the X-ray observations to map essentially the sources in the same configuration.

X-ray absorption variability has been observed on a large number of sources in time-scales as short as less than a day, including temporary 'eclipses' of otherwise unobscured objects (e.g. Elvis et al. 2004; Risaliti et al. 2005, 2011; Puccetti et al. 2007; Bianchi et al. 2009b). However, absorption on these scales, being well within the sublimation radius and hence dust free, cannot affect the reddening of the BLR. Therefore, this short-term variability could only explain the observation of an X-ray obscured Seyfert 1 galaxy (if observed when the cloud absorbs the X-ray source), but not the X-ray unabsorbed Sy2 galaxies we are interested in.

On the other hand, the BLR can only be reddened by an absorber at a distance greater than the dust sublimation radius, which can be roughly written as $r_{\rm d} \simeq 0.04\, L_{43}^{1/2}$ pc, with L_{43} being the bolometric luminosity in 10^{43} erg s^{-1} (adapted from Barvainis 1987). In order to cover the entire BLR, a cloud must have at least the same dimensions, which again can be roughly expressed as $r_{\rm b} \simeq 0.008\, L_{43}^{1/2}$ pc (adapted from the relationship for the Hβ line presented in Bentz et al. 2009). The minimum time $t_{\rm m}$ needed in order to completely cover or uncover the BLR is, therefore, the crossing time of such a cloud: $v = r_{\rm b}/t_{\rm m}$. Assuming that the cloud is in Keplerian motion around the central black hole (BH) at distance $r_{\rm d}$, we find an estimate of $t_{\rm m}$ as

$$t_{\rm m} = 7.9 \times 10^7\, L_{43}^{3/4}\, M_8^{-1/2}\ {\rm s}. \quad (1)$$

Therefore, even the $\simeq$6 month delay between the X-ray and optical observation in NGC 3660 is safely shorter than the minimum variability time-scale for a reddening change of the BLR estimated for this source, which is a few years from the above formula and the BH mass and bolometric luminosity reported in Section 5.3.

The optical long-slit spectrographs we used had a variety of spectral dispersions, typically dubbed 'intermediate', i.e. enough to measure the width of an emission line of several 100 km s^{-1} intrinsic width. Observations were done with the slit oriented in parallactic angle in order not to lose flux at bluer wavelengths. The data were reduced using standard processing techniques, including debiasing, flat-fielding along the spectral direction, arc lamp wavelength calibration, spectral extraction and background subtraction from the nearby sky and approximate flux rectification using spectrophotometric standard stars (but not correction for slit width). Statistical errors were properly propagated through the whole process, enabling us to perform statistical modelling of patches of the spectra, which we used to deblend and characterize emission lines. We typically took spectral regions around the Hβ λ4861 and [O III] λ5007 emission lines and the Hα λ6563 and [N II] λ6583 lines. Spectra were fitted, via χ^2 minimization, by modelling the continuum as a power law or a SPLINE function, and each line component as a Gaussian. In order to disentangle any broad component of Hα, we assumed that (i) F([N II] λ6583)/F([N II] λ6548) = 3, as required by the ratio of the respective Einstein coefficients, (ii) λ_2/λ_1 = 6583.39/6548.06 and (iii) the [N II] lines are Gaussians with the same width. With the above exception, the central wavelengths of all lines were left free, not constraining them to have a fixed ratio between them or to be at the expected redshift. The line flux ratios were then plotted in the diagrams shown in Fig. 1, where the separations between starburst galaxies, Seyfert galaxies and low-ionization nuclear emission-line regions (LINERs) are marked as in Kewley et al. (2006).

4 SPECTRAL ANALYSIS

4.1 IC 1631

The spectral classification of this source as given by Panessa & Bassani (2002) was rather ambiguous, because of the lack of a measured flux of [O I] 6300. Indeed, their optical data were taken from Sekiguchi & Wolstencroft (1993), who classified IC 1631 as

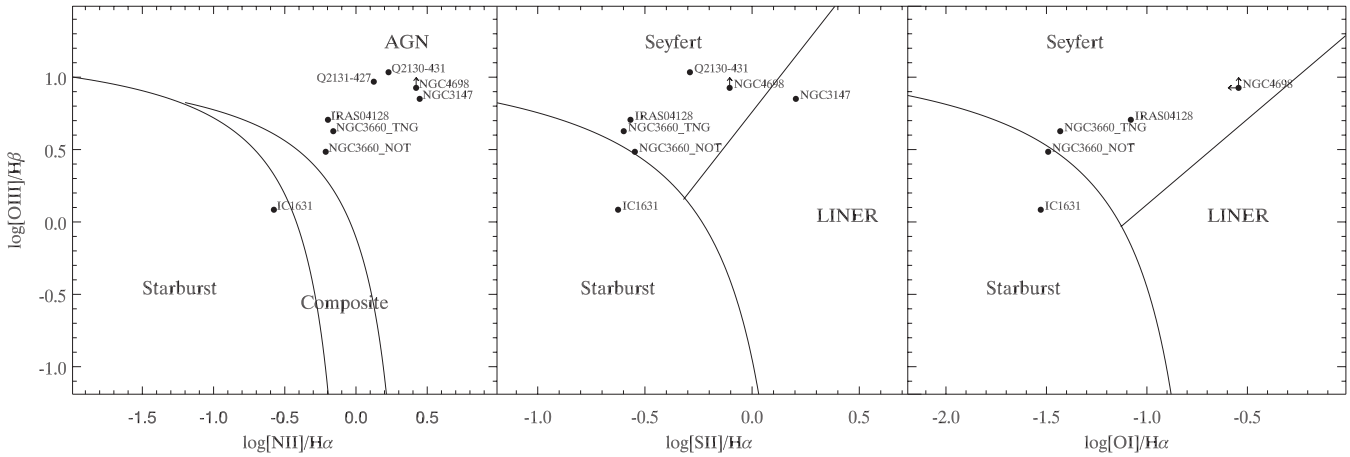

Figure 1. Optical line diagnostic diagrams from the analysis of the optical spectra of our campaign. Arrows indicate upper/lower limits. Classifications are done as in Kewley et al. (2006), and references therein (see Table 2).

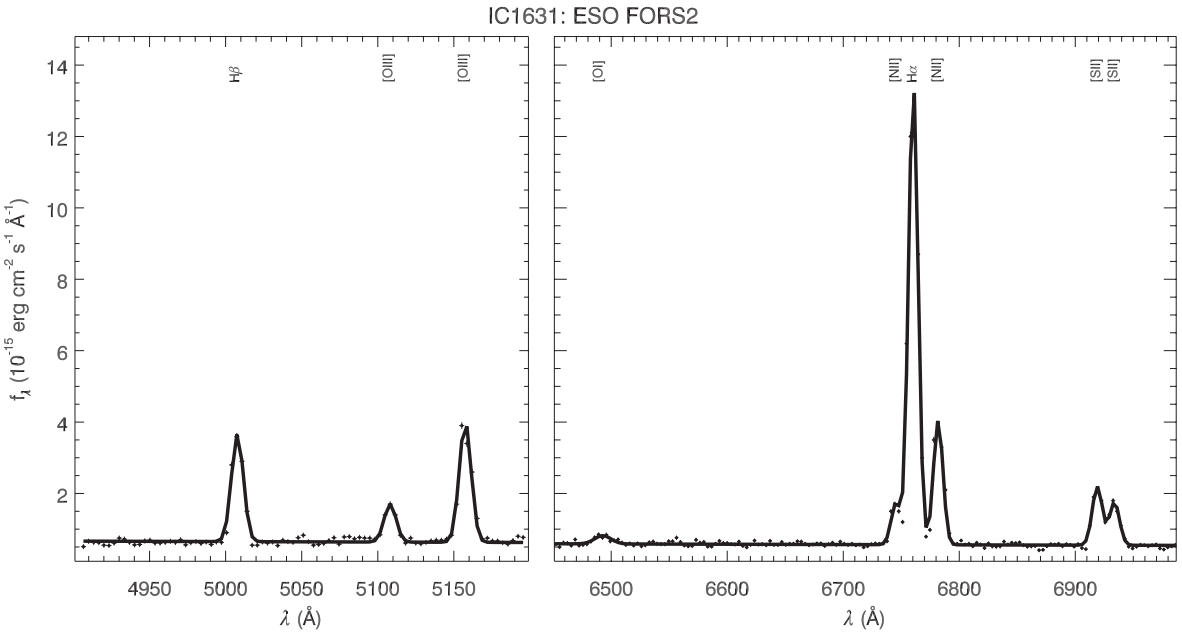

Figure 2. IC 1631: ESO optical spectrum and best fit (see Table 3).

a starburst galaxy. On the other hand, Kirhakos & Steiner (1990) opted for an AGN classification, based on the large full width at half-maximum (FWHM) of the [O III] line. The optical line ratios derived from our high-quality spectrum, shown in Fig. 2, all clearly point to a classification as a starburst galaxy (see Tables 2 and 3, and Fig. 1), with no sign of AGN activity in this galaxy.

In X-rays, IC 1631 had never been observed before our campaign, with the only exception of a non-detection by *Ginga*, with a very lose upper limit for the 2–10 keV flux of 1×10^{-11} erg cm^2 s^{-1}, as it was likely contaminated by Abell 2877 (Awaki & Koyama 1993). Although the source is quite faint, the *XMM–Newton* EPIC pn image appears extended, with roughly an excess in counts of 40–80 per cent with respect to the point spread function between 10 and 15 arcsec, and no variability is observed. The X-ray spectrum can be fitted ($\chi^2 = 14/13$ degree of freedom or d.o.f.) with a simple power law ($\Gamma = 2.0 \pm 0.3$), absorbed only by the Galactic column density (Fig. 3). Any absorption in excess, at the redshift of the source, can be constrained to be lower than 4×10^{20} cm^{-2}. No

Table 2. Optical line diagnostics from the analysis of the optical spectra of our campaign (ratios are expressed in decadic logarithms). Classifications (SB: Starburst; S1: Seyfert 1; S2: Seyfert 2) are done as in Kewley et al. (2006), and references therein (see Fig. 1).

Source	$\frac{[\mathrm{N\,II}]}{\mathrm{H}\alpha}$	$\frac{[\mathrm{O\,III}]}{\mathrm{H}\beta}$	$\frac{[\mathrm{S\,II}]}{\mathrm{H}\alpha}$	$\frac{[\mathrm{O\,I}]}{\mathrm{H}\alpha}$	Cl.
IC 1631	−0.58	0.08	−0.63	−1.53	SB
IRAS 01428−0404	−0.20	0.71	−0.57	−1.08	S2
Mrk 273x	–	0.85	–	–	S2?
NGC 3147	0.3	0.85	0.2	–	S2
NGC 3660 (NOT)	−0.21	0.48	−0.55	−1.49	S2
NGC 3660 (TNG)	−0.16	0.63	−0.60	−1.43	S2
NGC 4698	0.42	>0.93	−0.10	<−0.54	S2
Q2130−431	0.23	1.03	−0.29	–	S1
Q2131−427	0.12	0.97	–	–	S2

Table 3. IC 1631: optical emission lines in the European Southern Observatory (ESO) spectrum (see Fig. 2).

Line	λ_1	FWHM	Flux
(1)	(2)	(3)	(4)
Hβ	4861.33	490 ± 50	2.8 ± 0.3
[O III]	4958.92	540 ± 60	1.0 ± 0.2
[O III]	5006.85	540 ± 60	3.4 ± 0.4
[O I]	6300.32	1000 ± 700	0.4 ± 0.3
[N II]	6548.06	415 ± 40	1.19 ± 0.03
Hα	6562.79	414 ± 18	13.5 ± 0.6
[N II]	6583.39	415 ± 40	3.58 ± 0.09
[S II]	6716.42	430 ± 50	1.8 ± 0.3
[S II]	6730.78	430 ± 50	1.4 ± 0.3

Notes. Col. (1) Identification. (2) Laboratory wavelength (Å), in air (Bowen 1960). (3) km s^{-1} (instrumental resolution not removed). (4) 10^{-14} erg cm^{-2} s^{-1}.

iron line is required by the data, with an upper limit to its flux of 2×10^{-7} ph cm^{-2} s^{-1} in a local fit to the unbinned spectrum [due to the low level of continuum at this energy, no upper limit to the equivalent width (EW) can be estimated]. More refined models cannot be tested due to the low quality of the spectrum. However, the addition of a thermal component (APEC in XSPEC) gives a very good fit ($\chi^2 = 7/11$ d.o.f.) with $kT = 0.3^{+0.2}_{-0.1}$ keV and $\Gamma = 1.5 \pm 0.3$, in agreement with the expectations for starburst galaxies (e.g. Persic & Rephaeli 2002).

The 2–10 (0.5–2) keV flux is 3.0 ± 1.0 (2.3 ± 0.3) $\times 10^{-14}$ erg cm^{-2} s^{-1}, corresponding to a 2–10 keV luminosity of $6.6 \pm 2.1 \times 10^{40}$ erg s^{-1}. This luminosity would correspond to a star formation rate of $\simeq$10–15 M$_\odot$ yr^{-1}, according to the relations presented in Ranalli, Comastri & Setti (2003), which is well in the range of local starburst galaxies (e.g. Sargsyan & Weedman 2009).

4.2 IRAS 01428−0404

IRAS 01428−0404 was optically classified as Sy2 by Moran, Halpern & Helfand (1996) and Pietsch et al. (1998). In our new optical spectrum (Fig. 4), the line ratios all clearly confirm this classification (see Tables 2 and 4, and Fig. 1).

In X-rays, IRAS 01428−0404 was detected in the *ROSAT* All-Sky Survey (performed in the second half of 1990) with a 0.1–2.4 keV flux of 6.3×10^{-12} erg s^{-1} cm^{-2} (Boller et al. 1992), but the identification was subsequently dubbed as insecure by Boller et al. (1998), and by *ASCA* (in 1997) with a reported 2–10 keV flux of 4×10^{-13} erg s^{-1} cm^{-2} (Panessa & Bassani 2002). As for our *XMM–Newton* observation, the simplest possible model, i.e. a power law absorbed by the Galactic column density, provides a good fit (normalized Cash statistics is 39/36 d.o.f.) to the 0.5–8 keV spectrum (the source is not detected above this energy: see Fig. 5). The power-law index is $\Gamma = 2.3 \pm 0.3$, and no intrinsic absorption is found at the redshift of the source ($N_{\rm H} < 6 \times 10^{20}$ cm^{-2}). No significant variability is observed during the observation. The 2–10 (0.5–2) keV observed flux is 2.1 ± 0.5 (3.0 ± 0.5)$\times 10^{-14}$ erg s^{-1} cm^{-2}, corresponding to an absorption-corrected luminosity of 1.9 ± 0.4 (2.5 ± 0.4)$\times 10^{40}$ erg s^{-1}. The 2–10 keV to [O III] luminosity ratio, once corrected for the Balmer decrement as measured in our optical spectrum, is $\log \frac{L_{\rm X}}{L_{\rm [O\,III]}} \simeq -0.5$, strongly suggesting that the source is Compton thick (see e.g. Panessa et al. 2006; Lamastra et al. 2009; Marinucci et al. 2012). Although flatter power-law indices are expected for the X-ray spectra of Compton-thick sources, much steeper ones are usually found in low-count sources, since the dominating component is the soft excess which peaks where the instrumental effective area is larger, instead of the Compton reflection component at higher energies (see e.g. Bianchi et al. 2006).

This interpretation is also in agreement with the overall spectral energy distribution (SED), shown in the left-hand panel of Fig. 6, which resembles that of a Compton-thick source. The SED has been built using data from NED, SuperCosmos Sky Survey and our *XMM–Newton* proprietary data (photometric data from the optical monitor and re-binned X-ray spectrum). The SED is corrected for Galactic absorption and shifted to rest frame. We fitted this SED with a set of pure AGN and pure starburst templates (see Ruiz et al. 2010 for a complete description of these templates), finding as a best-fitting model a combination of a type 2 AGN and a starburst. The AGN template (NGC 3393) has a hydrogen column density $>10^{25}$ cm^{-2}. The starburst component (template from IRAS 12112+0305) is $\simeq$40 per cent of the total bolometric output of this source.

The only evidence potentially at odds with the Compton-thick interpretation of IRAS 01428−0404 is represented by the larger X-ray fluxes measured in the past *ASCA* observation. Therefore, we downloaded the *ASCA* data from the Tartarus data base,[1] and re-analysed the GIS and SIS spectra. The 0.5–2 keV energy band can be fitted with a very steep power law absorbed by the Galactic column density, for a flux in the same band of $(3.0 \pm 0.3) \times 10^{-13}$ erg s^{-1} cm^{-2}. In the 2–10 keV band, the source is undetected (3σ confidence level) by the SIS0 and the GIS2, while it is formally detected ($\simeq 4\sigma$) by the SIS1 and the GIS3. When fitted with a pure reflection component, we recover a 2–10 keV flux of $(2.3 \pm 1.0) \times 10^{-13}$ erg s^{-1} cm^{-2}. Both the soft and the hard X-ray fluxes are, therefore, roughly a factor of 10 larger than that in our *XMM–Newton* observation. However, in the *ASCA* source extraction region there are several other sources, four of them with a comparable X-ray flux to the target (see right-hand panel of Fig. 6). None of these sources have been identified yet. Their X-ray spectra can be fitted with a simple power law, absorbed by the Galactic column density. We give basic information and X-ray fluxes in Table 5 for each of them. The combined flux of these sources and IRAS 01428−0404 is consistent with the *ASCA* observed flux in the 2–10 keV band, while it is still a factor of 3 lower in the 0.5–2 keV

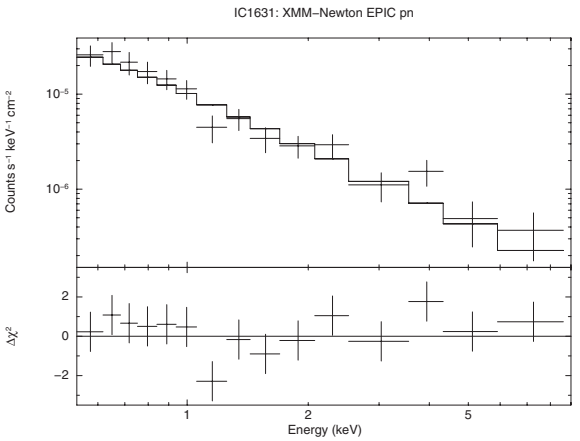

Figure 3. IC 1631: the *XMM–Newton* observation. EPIC pn spectrum, along with the best fit and residuals in terms of $\Delta\chi^2$. See the text for details.

[1] http://tartarus.gsfc.nasa.gov

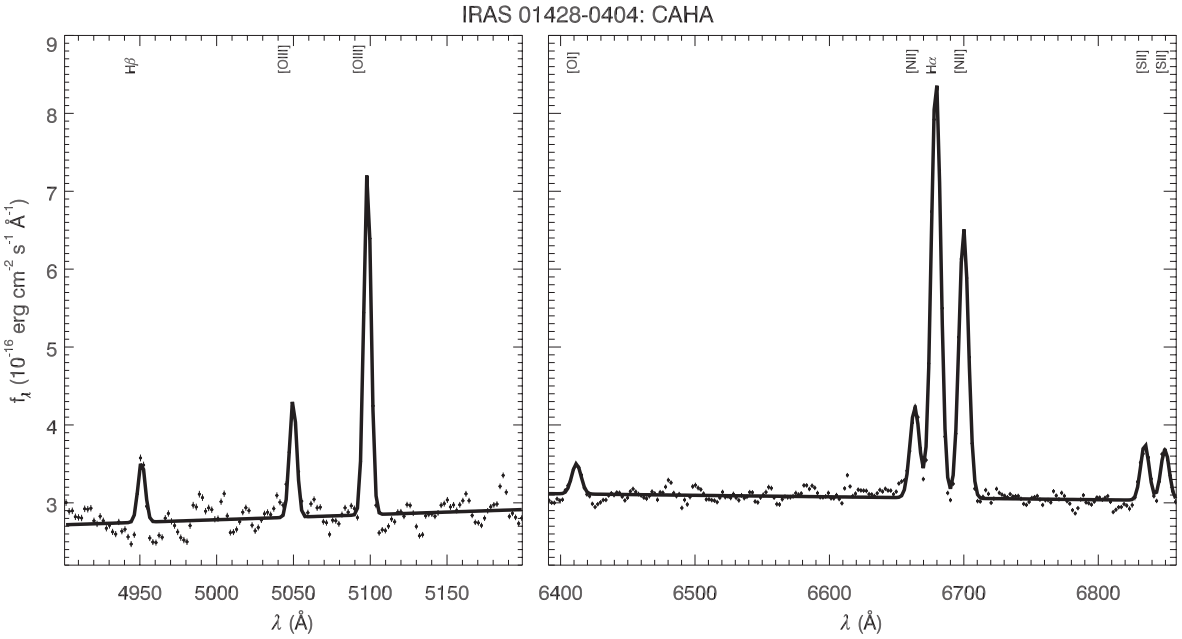

Figure 4. IRAS 01428−0404: CAHA optical spectrum and best fit (see Table 4).

Table 4. IRAS 01428−0404: optical emission lines in the CAHA spectrum (see Fig. 4).

Line (1)	λ_l (2)	FWHM (3)	Flux (4)
Hβ	4861.33	275 ± 15	5.2 ± 0.3
[O III]	4958.92	318 ± 4	8.7 ± 0.3
[O III]	5006.85	318 ± 4	26.4 ± 0.4
[O I]	6300.32	400 ± 30	3.9 ± 0.3
[N II]	6548.06	360 ± 4	9.92 ± 0.12
Hα	6562.79	364 ± 3	46.9 ± 0.4
[N II]	6583.39	360 ± 4	29.8 ± 0.4
[S II]	6716.42	345 ± 11	6.6 ± 0.4
[S II]	6730.78	345 ± 11	6.1 ± 0.3

Notes. Col. (1) Identification. (2) Laboratory wavelength (Å), in air (Bowen 1960). (3) km s^{-1} (instrumental resolution not removed). (4) 10^{-16} erg cm^{-2} s^{-1}.

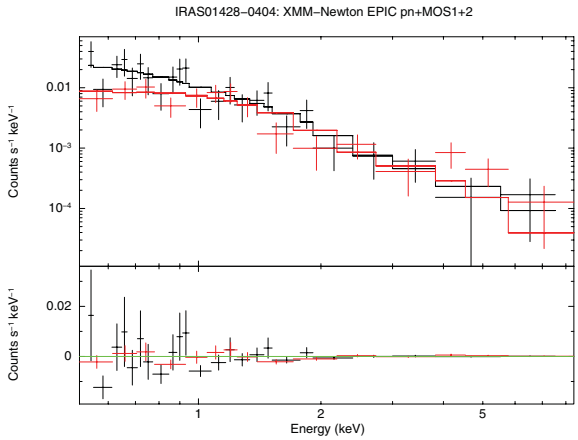

Figure 5. IRAS 01428−0404: the *XMM–Newton* observation. EPIC pn (black) and co-added MOS (red) spectra, along with the best fit and residuals. See the text for details.

band. However, there is no reason to assume that the varying source is IRAS 01428−0404.

4.3 Mrk 273x

Mrk 273x was classified as a Sy2 galaxy by Xia et al. (1999) on the basis of the large FWHM of the [O III] emission line and the ratio [O III] 5007/Hβ $>$ 3. Unfortunately, during our optical observation the source was observed very close to morning twilight with very large fringing and some sort of electronic noise, so the spectrum is rather less than optimal, making it difficult to exclude the presence of a broad component of Hβ. Moreover, the redshift of the source (0.458) only allowed us to observe the [O III] 5007 and Hβ wavelength range, thus limiting our diagnostics (Fig. 7). Therefore, we can basically confirm the results presented by Xia et al. (1999), without shedding more details on the optical classification of the source and the presence of broad components of the permitted lines (see Tables 2 and 6). A spectrum encompassing the Hα emission line region is needed to settle the issue.

In X-rays, *ASCA* and *BeppoSAX* could not spatially resolve Mrk 273x from the neighbour Mrk 273 (Iwasawa 1999; Risaliti et al. 2000). Subsequent observations with *Chandra*, *XMM–Newton* and *Suzaku* provided an unabsorbed power-law spectrum, with a large luminosity ($\simeq 10^{44}$ erg s^{-1}) and small variability on short and long time-scales (Xia et al. 2002; Balestra et al. 2005; Teng et al. 2009). Our *XMM–Newton* observation was divided into four distinct exposures, all plagued by very high particle background. Even after the optimization method described in Section 3.1, the resulting spectrum is very poor (see Fig. 8), and can be fitted by a simple power law ($\Gamma = 1.6^{+0.5}_{-0.4}$) absorbed by the Galactic column density ($\chi^2 = 17/20$ d.o.f.). Any absorption in excess, at the redshift of the source, can be constrained to be lower than 2×10^{21} cm^{-2}. A more stringent upper limit (4.5×10^{20} cm^{-2}) was found by Balestra et al. (2005) with the previous *XMM–Newton* observation. The 2–10 (0.5–2) keV

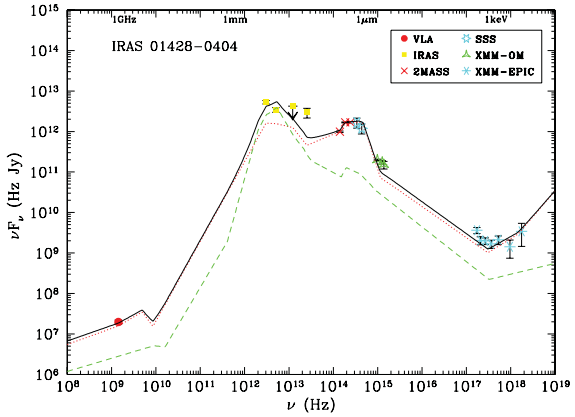

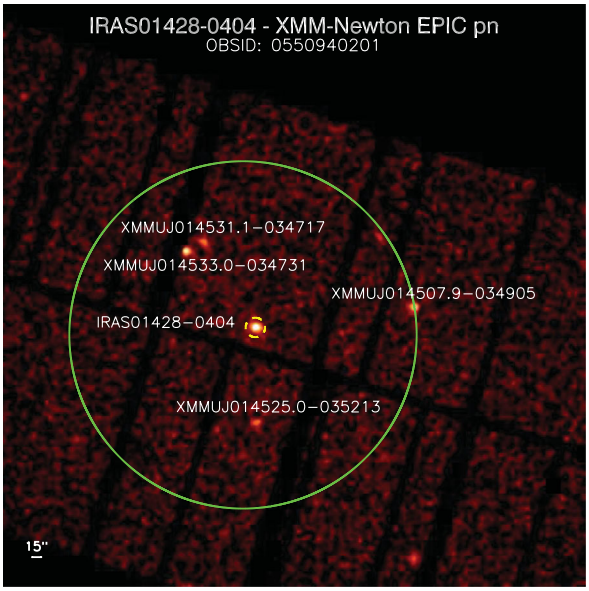

Figure 6. Left: SED of IRAS 01428−0404 and best-fitting model (black solid line). The red-dotted line is the AGN component and the green-dashed line is the starburst component. See the text for details. Right: *XMM–Newton* EPIC pn field of IRAS 01428−0404. The extraction region for the pn spectrum is shown in yellow. The large green circle is the extraction region for the *ASCA* SIS1 spectrum, which includes several other bright sources (see Table 5).

Table 5. List of unidentified X-ray sources detected in the *XMM–Newton* observation of IRAS 01428−0404, within the source extraction region adopted for the *ASCA* observation. See right-hand panel of Fig. 6 and the text for details.

Source (1)	RA (2)	Dec. (3)	Γ (4)	F_s (5)	F_h (6)
XMMU J014507.9−034905	01:45:07.9	−03:49:05.8	$1.6^{+0.2}_{-0.3}$	2.5 ± 0.4	6.1 ± 0.7
XMMU J014525.0−035213	01:45:25.0	−03:52:13.0	$1.8^{+0.6}_{-0.5}$	1.0 ± 0.3	1.8 ± 0.5
XMMU J014531.1−034717	01:45:31.1	−03:47:17.0	2.1 ± 0.6	1.1 ± 0.3	1.1 ± 0.2
XMMU J014533.0−034731	01:45:33.0	−03:47:31.4	$1.6^{+0.4}_{-0.3}$	1.9 ± 0.4	4.8 ± 1.9

Notes. Col. (1) Name of the source following the naming conventions suggested by the *XMM–Newton* team. (2), (3) RA and Dec. (equatorial J2000). (4) X-ray photon index. (5), (6) 0.5–2 and 2–10 keV fluxes are in 10^{-14} erg s^{-1} cm^{-2}.

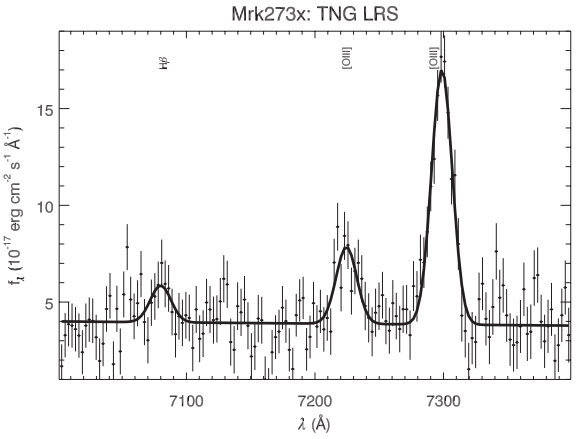

Figure 7. Mrk 273x: TNG spectrum and best fit (see Table 6).

Table 6. Mrk 273x: optical emission lines in the TNG LRS spectrum (see Fig. 7).

Line (1)	λ_l (2)	FWHM (3)	Flux (4)
Hβ	4861.33	800 ± 80	3.8 ± 1.9
[O III]	4958.92	800 ± 80	8 ± 2
[O III]	5006.85	800 ± 80	27 ± 3

Notes. Col. (1) Identification. (2) Laboratory wavelength (Å), in air (Bowen 1960). (3) km s^{-1} (instrumental resolution not removed). (4) 10^{-16} erg cm^{-2} s^{-1}.

flux is 1.1 ± 0.6 (0.45 ± 0.09) × 10^{-13} erg cm^{-2} s^{-1}, corresponding to a 2–10 (0.5–2) keV luminosity of 7.3 ± 2.9 (3.0 ± 0.6) × 10^{43} erg s^{-1}. The 2–10 keV to [O III] luminosity ratio is, therefore, $\log \frac{L_X}{L_{[O\,III]}} \simeq 1.6$, which is perfectly consistent with the source being unobscured (see e.g. Lamastra et al. 2009), even considering the (unknown, due to the lack of the Hα emission line in the optical spectrum) Balmer decrement to be applied to correct for reddening the [O III] luminosity.

4.4 NGC 3147

The classification of NGC 3147 as a Sy2 was originally given by Ho, Filippenko & Sargent (1997a). *ASCA* provided the first X-ray spectrum, without significant absorption, as later confirmed by *BeppoSAX* (Dadina 2007) and *Chandra*, which also showed that no off-nuclear source can significantly contribute to the nuclear

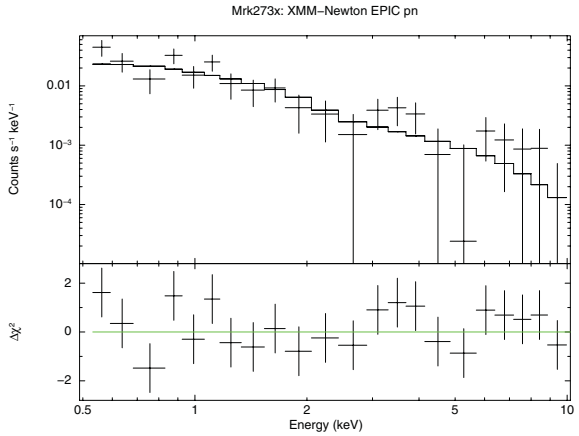

Figure 8. Mrk 273x: the *XMM–Newton* observation. EPIC pn spectrum, along with the best fit and residuals in terms of $\Delta\chi^2$. See the text for details.

emission (Terashima & Wilson 2003). The simultaneous X-rays and optical observations of NGC 3147 were analysed in detail by Bianchi et al. (2008), who confirmed the lack of broad permitted lines in the optical spectrum and X-ray absorption, strongly suggesting that the source is a 'true type' Sy2. These conclusions were further refined thanks to a long broad-band *Suzaku* observation, which allows only for a peculiar Compton-thick source dominated by a highly ionized and compact reflector as a viable alternative (Matt et al. 2012). However, this solution is strongly disfavoured by the observed X-ray variability on yearly time-scales of the source. That the variation cannot be due to a confusing source is demonstrated by the fact that the highest flux has been measured by the best spatial resolution satellite (e.g. Matt et al. 2012, and references therein). This again leaves the 'true' Sy2 nature of NGC 3147 as the most likely explanation.

4.5 NGC 3660

NGC 3660 was optically classified as a Sy2 by Moran et al. (1996) and Gu et al. (2006), but as a composite/transition Sy2/starburst galaxy by Kollatschny et al. (1983), Contini, Considere & Davoust (1998) and Gonçalves, Véron-Cetty & Véron (1999). This could be due to the presence of a very compact nuclear starburst detected through the 3.3 μm polycyclic aromatic hydrocarbon emission feature (Imanishi 2003). A weak broad component of the Hα and/or the Hβ line was reported by Kollatschny et al. (1983), Gonçalves et al. (1999) and Cid Fernandes et al. (2004), after removal of the starlight. We show in Fig. 9 our new optical spectra: the optical line ratios are more typical of a Seyfert galaxy, but we confirm the possible contamination by a starburst region, mostly in the NOT spectrum (see Tables 2, 7 and 8 and Fig. 1). Both spectra also confirm the possible presence of a broad (FWHM $\simeq 3000\,\mathrm{km\,s^{-1}}$) component of the H$\alpha$ emission line, but with a flux at most 0.7 (0.8) that of the narrow core, in the NOT (TNG) spectrum. Fitting a component with the same width at the Hβ wavelength results in an upper limit to the flux of only 0.1 (0.5) with respect to the narrow core.

In order to confirm or reject the signatures of a (weak or heavily reddened) BLR in the optical spectrum, we also observed NGC 3660 in the near-infrared (NIR), with two different grisms. There is no detection of any broad permitted hydrogen Paschen lines in either spectra (see Fig. 10 and Table 9). In particular, the tightest upper limit on a broad component of Paβ (once fixed the FWHM to the one possibly found in the optical spectra) comes from the spectrum with the highest resolution: its flux is at most 0.4 that of the narrow component. Therefore, we conclude that the BLR is not visible in the infrared (IR), and the weak broad component possibly detected in the optical spectra is likely an artefact of a bad modelling of the continuum.

Table 7. NGC 3660: optical emission lines in the NOT spectrum (see Fig. 9).

Line	λ_l	FWHM	Flux
(1)	(2)	(3)	(4)
Hβ	4861.33	250 ± 30	3.8 ± 0.4
[O III]	4958.92	280 ± 10	4.0 ± 0.3
[O III]	5006.85	280 ± 10	11.6 ± 0.5
[O I]	6300.32	240 ± 110	0.5 ± 0.2
[N II]	6548.06	200 ± 10	3.17 ± 0.13
Hα	6562.79	200 ± 10	15.5 ± 0.5
Hα	6562.79	2900 ± 500	9.5 ± 1.4
[N II]	6583.39	200 ± 10	9.5 ± 0.4
[S II]	6716.42	200 ± 20	2.5 ± 0.3
[S II]	6730.78	200 ± 20	1.9 ± 0.2

Notes. Col. (1) Identification. (2) Laboratory wavelength (Å), in air (Bowen 1960). (3) km s^{-1} (instrumental resolution not removed). (4) 10^{-15} erg cm^{-2} s^{-1}.

Table 8. NGC 3660: optical emission lines in the TNG spectrum (see Fig. 9).

Line	λ_l	FWHM	Flux
(1)	(2)	(3)	(4)
Hβ	4861.33	520 ± 100	5.1 ± 0.8
[O III]	4958.92	510 ± 20	7.7 ± 0.6
[O III]	5006.85	510 ± 20	21.6 ± 0.7
[O I]	6300.32	370[a]	1.0 ± 0.6
[N II]	6548.06	420 ± 20	6.2 ± 0.2
Hα	6562.79	440 ± 20	27.0 ± 0.8
Hα	6562.79	2700 ± 300	18.7 ± 2.5
[N II]	6583.39	420 ± 20	18.7 ± 0.7
[S II]	6716.42	340 ± 50	3.1 ± 0.6
[S II]	6730.78	340 ± 50	3.7 ± 0.6

Notes. Col. (1) Identification. (2) Laboratory wavelength (Å), in air (Bowen 1960). (3) km s^{-1} (instrumental resolution not removed). (4) 10^{-15} erg cm^{-2} s^{-1}.
[a]Frozen in the fit.

In X-rays, NGC 3660 was detected in the *ROSAT* All-Sky Survey with a 0.1–2.4 keV flux of 1.4×10^{-12} erg s^{-1} cm^{-2} (Boller et al. 1992). The *ASCA* spectrum is fitted well by a power law with no absorption above the Galactic column, for a 2–10 keV flux of 2.3×10^{-12} erg s^{-1} cm^{-2} (Brightman & Nandra 2008). Interestingly, the same authors report a significant variability on short time-scales. The *BeppoSAX* data confirm the absence of absorption in excess to that of the Galaxy, but the 20–100 keV flux measured by the PDS is well above what is predicted by extrapolating the spectrum observed below 10 keV, suggesting a Compton-thick absorber along the line of sight, although at odds with the upper limit on the EW of the iron Kα line of 230 eV (Dadina 2007). Moreover, the source is not detected by the *Swift* BAT hard X-ray survey, even if the reported *BeppoSAX* PDS flux is larger than its flux limit (Cusumano et al. 2010).

Our *XMM–Newton* data confirm the rapid variability of NGC 3660 both in the soft and in the hard X-rays, with no strong hints for variations of the hardness ratio (see the left-hand panel of

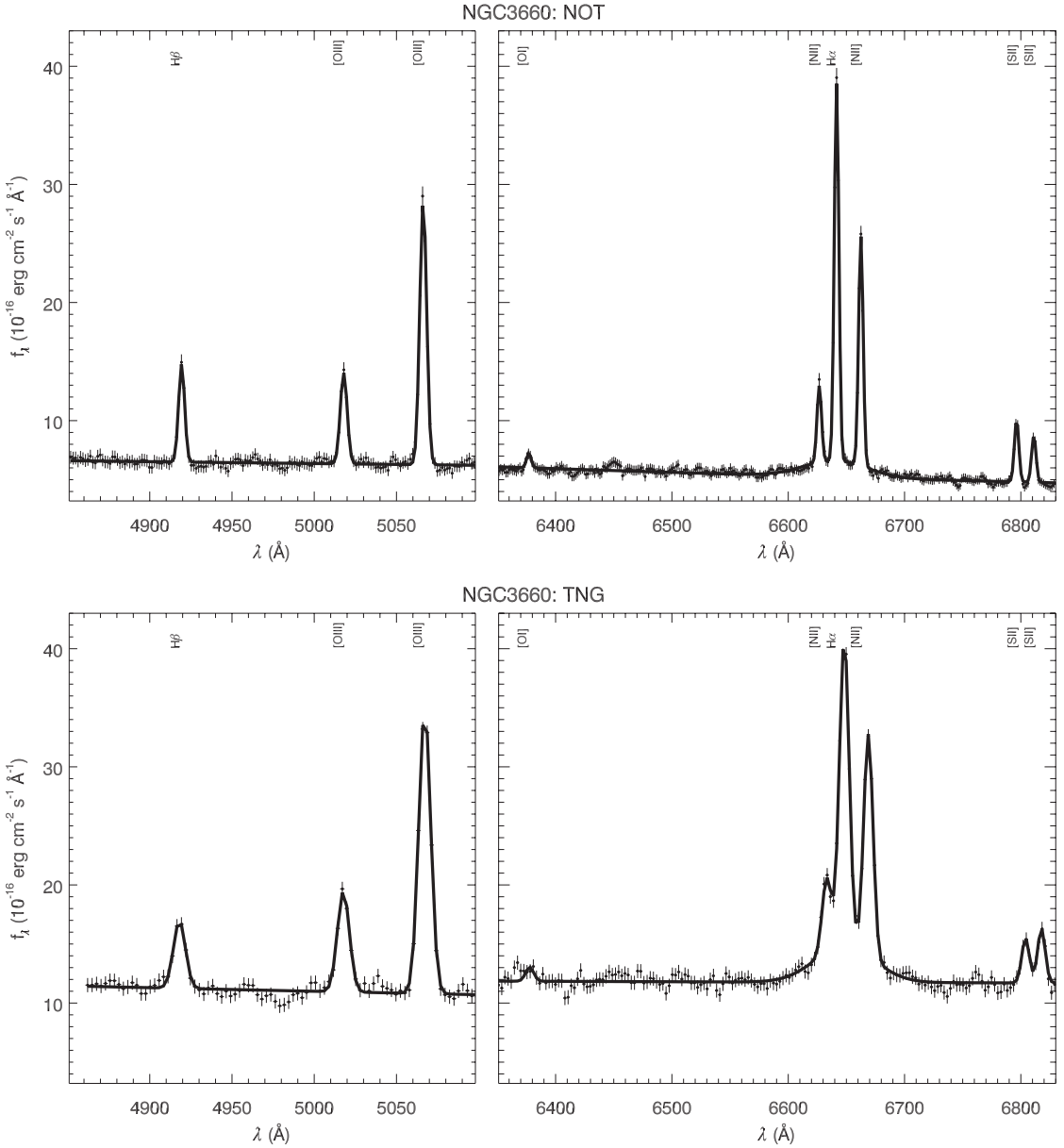

Figure 9. NGC 3660: NOT and TNG optical spectra along with best fits (see Tables 7 and 8).

Fig. 11). The EPIC pn and co-added MOS spectra cannot be fitted by a simple power law absorbed by the Galactic column density ($\chi^2 = 535/281$ d.o.f.), mainly due to a clear excess below 0.8 keV. The latter can be modelled by a blackbody emission, at a temperature of $T = 0.082 \pm 0.008$ keV, resulting in an acceptable fit ($\chi^2 = 310/279$ d.o.f.), with a power-law index $\Gamma = 1.99 \pm 0.03$. The addition of a neutral iron Kα narrow ($\sigma = 0$ eV) emission line at an energy fixed to 6.4 keV produces a marginal improvement of the fit ($\Delta\chi^2 = 4$ for one less d.o.f.). Its flux is $(1.8 \pm 1.5) \times 10^{-6}$ ph cm^{-2} s^{-1}, and EW $= 60 \pm 50$ eV. A further improvement is achieved by adding a Compton reflection component (modelled with PEXRAV, with the photon index tied to that of the primary power law, the inclination angle fixed to 30° and no cutoff energy), without changing significantly the other parameters, with the exception of the iron line, whose flux is now an upper limit ($<2.3 \times 10^{-6}$), and a rather unconstrained Compton reflection fraction ($R = 2.4 \pm 1.1$). The fit is now perfectly acceptable ($\chi^2 = 291/277$ d.o.f.) and is shown in the right-hand panel of Fig. 11. The 0.5–2 keV flux is $(2.45 \pm 0.05) \times 10^{-12}$ erg s^{-1} cm^{-2}, while the 2–10 keV flux is $(3.09 \pm 0.05) \times 10^{-12}$ erg s^{-1} cm^{-2}. They correspond to luminosities of $(9.5 \pm 0.2) \times 10^{41}$ erg s^{-1} and $(1.03 \pm 0.02) \times 10^{42}$ erg s^{-1}, respectively.

4.6 NGC 4698

NGC 4698 was classified as a Sy2, with no trace of broad Hα, by Ho et al. (1997a); Ho et al. (1997b). Our optical spectrum, shown in Fig. 12, confirms unambiguously this classification (see Table 10 and Fig. 1).

In X-rays, after the detection by *Einstein* (Fabbiano, Kim & Trinchieri 1992), NGC 4698 was observed with *ASCA*, with a reported 2–10 keV luminosity of 2.2×10^{40} erg s^{-1}, and an upper limit of the order of 10^{21} cm^{-2} to any neutral absorbing column density (Pappa et al. 2001). The high spatial resolution of *Chandra* showed that the *ASCA* spectrum was dominated by two nearby

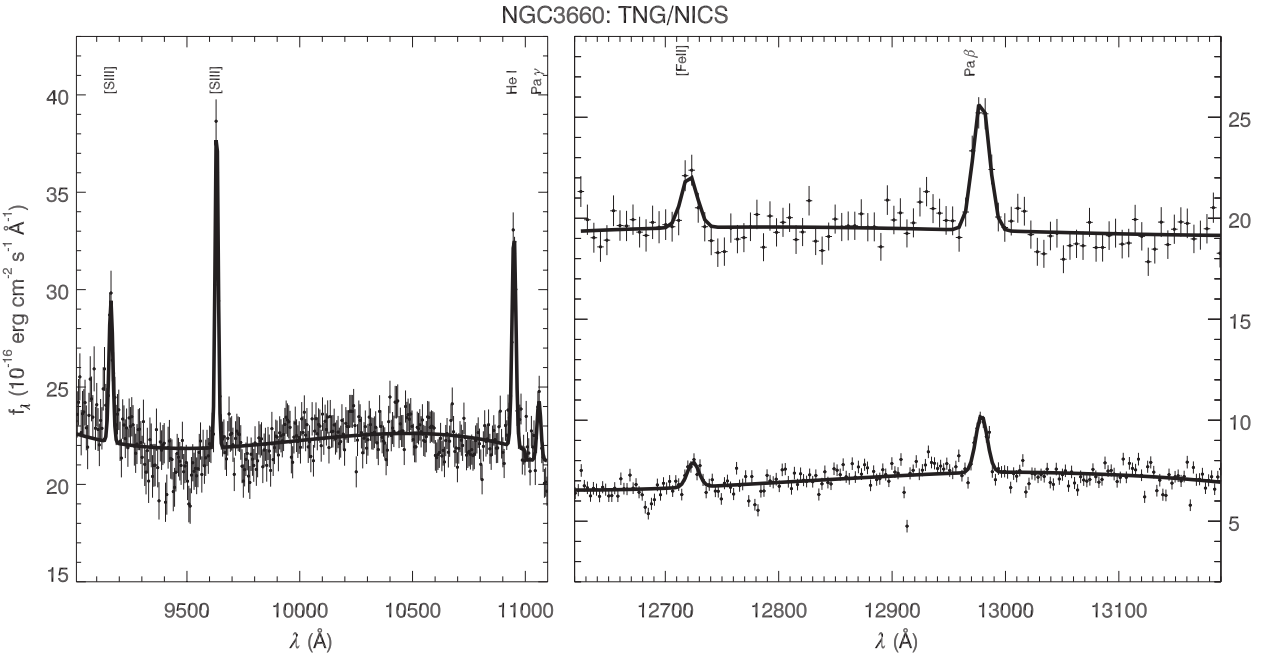

Figure 10. NGC 3660: TNG/NICS spectra. The left-hand panel shows the spectrum taken with grism IJ, while the right-hand panel shows both the IJ (upper spectrum) and the JS (lower spectrum, re-scaled for illustration purposes).

Table 9. NGC 3660: NIR emission lines in the TNG NICS spectrum with grism IJ (see Fig. 10).

Line	λ_l	FWHM	Flux
(1)	(2)	(3)	(4)
[S III]	9068.6	490 ± 50	12.7 ± 2.3
[S III]	9530.6	490 ± 50	28.0 ± 2.4
He I	10830.3	490 ± 60	22.0 ± 2.2
Pa γ	10938.1	490 ± 60	3.8 ± 1.7
[Fe II]	12566.8	360 ± 60	5.8 ± 1.5
Pa β	12818.1	360 ± 60	10.4 ± 2.1

Notes. Col. (1) Identification. (2) Laboratory wavelength (Å), in air (NIST Atomic Spectra Database. ver. 4.1.0): http://physics.nist.gov/asd (3) km s^{-1} (instrumental resolution not removed). (4) 10^{-15} erg cm^{-2} s^{-1}.

AGN, while the nuclear source has a significantly lower luminosity of 10^{39} erg s^{-1} (0.3–8 keV; Georgantopoulos & Zezas 2003). However, the nuclear spectrum is still unabsorbed ($N_H \simeq 5 \times 10^{20}$ cm^{-2}). These results were confirmed by the *XMM–Newton* observation, even if the source extraction region was partly contaminated by some off-nuclear sources in the host galaxy (Cappi et al. 2006; González-Martín et al. 2009).

We show in Fig. 13 the EPIC pn fields of the old and our *XMM–Newton* observations. As already shown by past works, the *ASCA* extraction region is significantly contaminated, while the *XMM–Newton* region that we chose contains ≃3 off-nuclear sources, whose total X-ray flux contribute to ≃40 per cent of the observed flux in that region, assuming the fluxes reported by Georgantopoulos & Zezas (2003). After having verified that there is no significant variability during the observations and the spectra extracted from that region are consistent between the two observations, we decided to co-add them. The resulting X-ray spectrum (shown in Fig. 14)

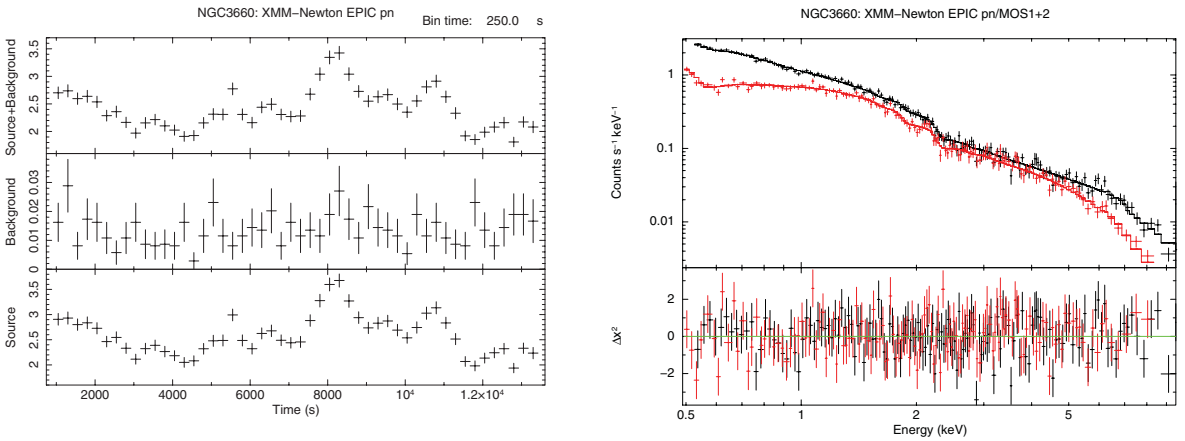

Figure 11. NGC 3660: the *XMM–Newton* observation. Left: EPIC pn light curve in the full band (0.3–10 keV). Right: EPIC pn (black) and co-added MOS (red) spectra, along with the best fit and residuals in terms of $\Delta\chi^2$. See the text for details.

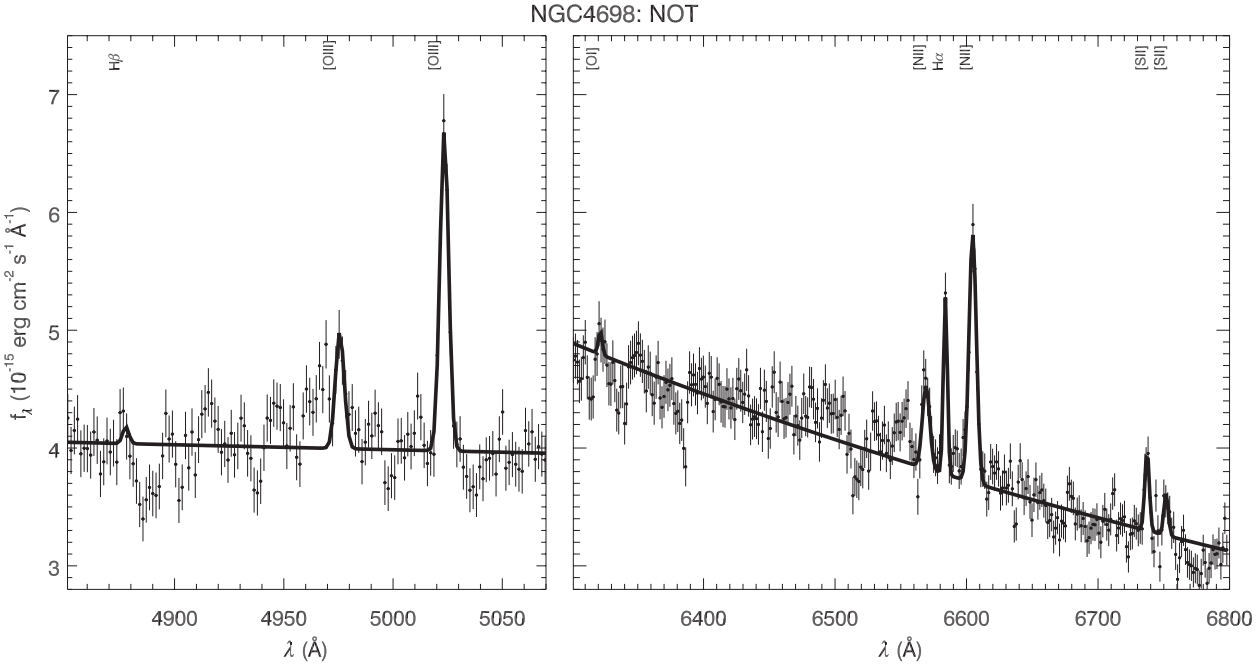

Figure 12. NGC 4698: NOT optical spectrum along with best fit (see Table 10).

Table 10. NGC 4698: optical emission lines in the NOT spectrum (see Fig. 12).

Line (1)	λ_l (2)	FWHM (3)	Flux (4)
Hβ	4861.33	270[a]	<1.6
[O III]	4958.92	270 ± 30	4.9 ± 1.2
[O III]	5006.85	270 ± 30	13.5 ± 1.4
[O I]	6300.32	150[a]	<1.6
[N II]	6548.06	300 ± 30	4.9 ± 0.4
Hα	6562.79	150 ± 30	5.6 ± 1.0
[N II]	6583.39	300 ± 30	14.8 ± 1.3
[S II]	6716.42	170 ± 50	2.9 ± 0.8
[S II]	6730.78	170 ± 50	1.5 ± 0.7

Notes. Col. (1) Identification. (2) Laboratory wavelength (Å), in air (Bowen 1960). (3) km s^{-1} (instrumental resolution not removed). (4) 10^{-15} erg cm^{-2} s^{-1}.
[a]Frozen in the fit.

is well fitted by a power law ($\Gamma = 1.90 \pm 0.10$) absorbed by the Galactic column density (normalized Cash = 146/126 d.o.f.). Only upper limits can be recovered for a local neutral absorbing column density ($N_H < 1.9 \times 10^{20}$) and an iron Kα emission line (EW < 450 eV). The 0.5–2 keV flux is $(2.1 \pm 0.4) \times 10^{-14}$ erg s^{-1} cm^{-2}, while the 2–10 keV flux is $(3.0 \pm 0.5) \times 10^{-14}$ erg s^{-1} cm^{-2}. They correspond to luminosities of $(5.3 \pm 0.9) \times 10^{38}$ and $(7.5 \pm 1.3) \times 10^{38}$ erg s^{-1}, respectively. The 2–10 keV to [O III] luminosity ratio is $\log \frac{L_X}{L_{[O\,III]}} < 0.15$, which is significantly lower than the average value for Compton-thin sources (see e.g. Lamastra et al. 2009). Moreover, this ratio is an upper limit for two reasons: first, because Hβ is not detected in our optical spectrum, so we only have a lower limit of the Balmer decrement and, therefore, to the intrinsic [O III] flux; moreover, the X-ray flux is an upper limit to the nuclear flux, which is likely to be contaminated by the off-nuclear sources detected by *Chandra*. We can derive a better estimate of the ratio by using the *Chandra* X-ray flux (taken from Georgantopoulos & Zezas 2003, but re-scaled to 2–10 keV), and the [O III] flux and Balmer decrement measured by Ho et al. (1997b). The resulting ratio is $\log \frac{L_X}{L_{[O\,III]}} = -0.27$, suggesting that the source is Compton thick (see e.g. Lamastra et al. 2009; Marinucci et al. 2012). This is in agreement with the low $L_X/L_{12\,\mu m}$ ratio, as reported by Shi et al. (2010).

4.6.1 The off-nuclear sources in the NGC 4698 field

As a final note, it is interesting to mention the large variability of the off-nuclear sources between the two *XMM–Newton* observations, as clearly shown in Fig. 13. In particular, the two sources inside the D_{25} of the galaxy that we label XMMU J124820.8+082918 and XMMU J124823.1+082802 are detected at high significance in the second observation, but not in the previous one. The fit with a simple power law with Galactic intervening absorption is acceptable for both objects ($\chi^2 = 30/31$ d.o.f. and 32/26 d.o.f., respectively), while more complicated spectral shapes are not required (see Table 11). The luminosities of the two sources ($\simeq 10^{39}$ erg s^{-1} if at the distance of NGC 4698) put them in the ULX regime, even if at the lower L_X range. We can interpret these sources as variable X-ray binaries with a BH mass of the order of $\simeq 10\,M_\odot$.

In the first *XMM–Newton* observation, at the positions of these two sources we find only upper limits to the luminosities of $\simeq 5$ and $\simeq 3 \times 10^{38}$ erg s^{-1}, respectively. XMMU J124820.8+082918 is marginally detected in the *Chandra* observation (performed one year later, in 2002) with a luminosity of $\simeq 3 \times 10^{37}$ erg s^{-1} (estimated by re-scaling its net counts with respect to the net counts in the nucleus as reported in table 1 of Georgantopoulos & Zezas 2003). On the other hand, XMMU J124823.1+082802 is not detected even in the *Chandra* observation, and might be a 'new' source. It is indeed consistent with a possible supernova (SN), both on energetics and spectral shape, since it can be fitted by an APEC thermal component (as for Type IIn SN, for instance, see e.g. Immler & Lewin 2003), although the fit cannot be statistically preferred to a simple power law.

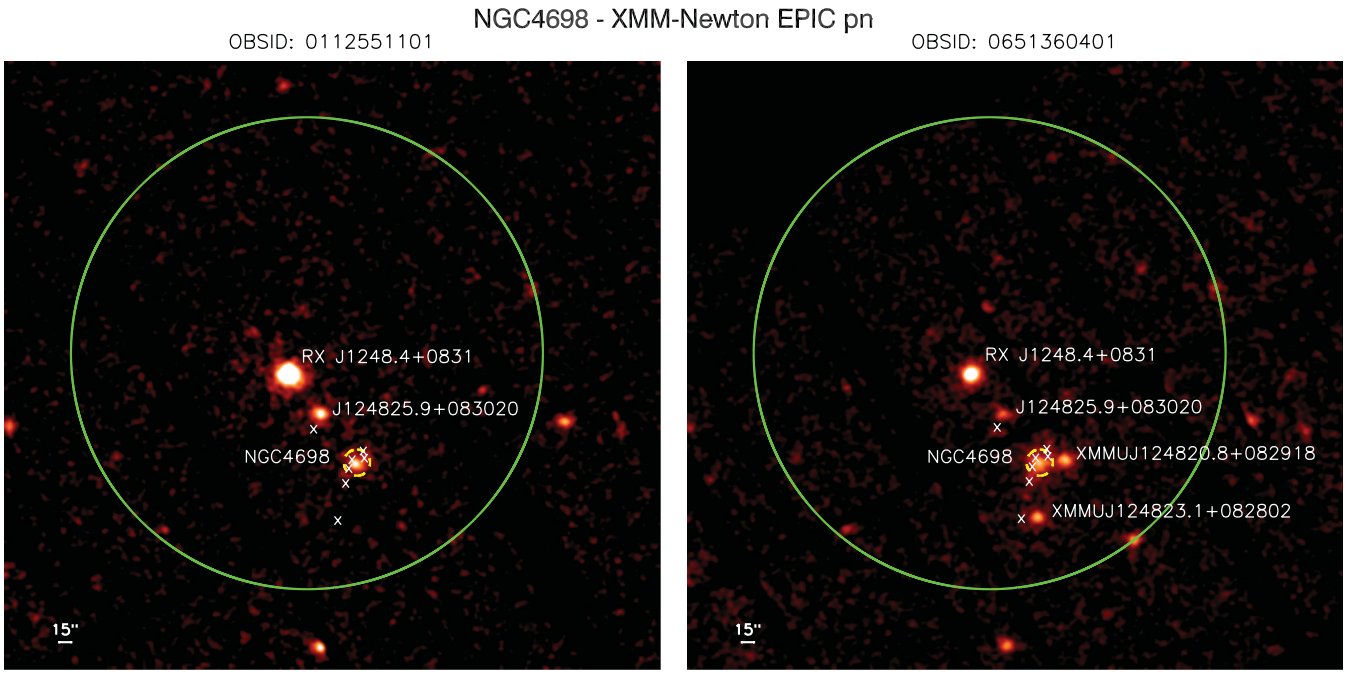

Figure 13. NGC 4698: *XMM–Newton* EPIC pn fields for the two observations. The extraction regions for the pn spectra are shown in yellow. The large green circle is the extraction region for the *ASCA* SIS0 spectrum. The white crosses are the sources detected in the *Chandra* observation, apart from NGC 4698, RX J1248.4+0831 and J124825.9+083020 (Georgantopoulos & Zezas 2003). The two ULXs appeared in the second observation (see the text and Table 11 for details) are marked in the right-hand panel.

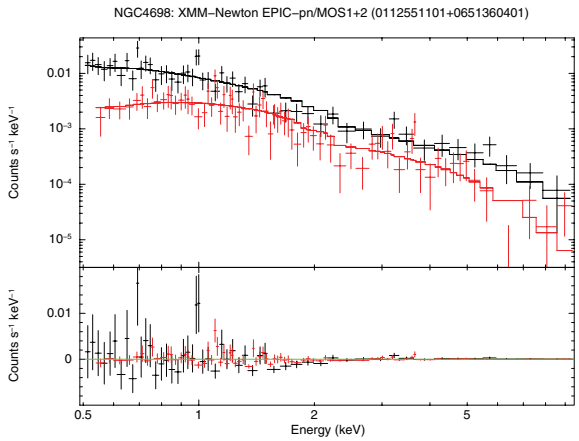

Figure 14. NGC 4698: EPIC pn (black) and co-added MOS (red) spectra, along with the best fit and residuals, for the combined *XMM–Newton* observations. See the text for details.

No apparent optical counterpart is present on the available optical/IR/ultraviolet (UV) material; however, none is from the epoch of the second *XMM–Newton* observation. ULXs are massive and therefore have young progenitors. It follows that the brightening or appearance of new sources is at odds with the optical classification of the nucleus of NGC 4698 with a population of age $T > 5$ Gyr (Corsini et al. 2012). We might speculate that the merging responsible for the nuclear appearance still has an impact on the outskirts of the galaxy, where star formation is visible in two UV rings from *GALEX* images (Cortese & Hughes 2009) at a rate of $\sim$0.1 $M_\odot$ yr^{-1} (De Looze, private communication), or that other mechanisms are at work.

4.7 Q2130−431 and Q2131−427

Q2130−431 and Q2131−427 belong to the 'naked' AGN class, where the absence of broad emission lines is accompanied by strong optical variability, suggesting that the nucleus is seen directly (Hawkins 2004). The absence of significant absorption in the X-ray spectra was later confirmed by *Chandra* snapshots (Gliozzi et al. 2007). The simultaneous X-rays and optical observations of Q2130−431 and Q2131−427 were analysed in detail by Panessa et al. (2009). While the optical spectrum of Q2130−431 do show broad components of the Balmer lines, Q2131−427 appears to lack broad optical lines and X-ray absorption along the line of sight, thus being a true type 2 Seyfert galaxy.

5 DISCUSSION

5.1 Rejected candidates: IC 1631, IRAS 01428−0404, NGC 4698 and Q2130−431

The Sy2 nature was confirmed by our new optical spectra for all the sources of our sample (but see Sections 4.3 and 5.2 for the case of Mrk 273x), with the exception of IC 1631 and Q2130−431. The classification of IC 1631 was ambiguous in the literature, but all the line diagnostics derived from our optical spectrum clearly put the source in the region populated by starburst galaxies. The X-ray data are consistent with this interpretation, requiring a star formation rate of $\simeq$10–15 $M_\odot$ yr^{-1}. Therefore, IC 1631 must be removed, once and for all, as an unabsorbed Sy2 candidate.

On the other hand, Q2130−431 clearly shows broad components of the Balmer lines in its optical spectrum. However, notwithstanding the negligible observed Balmer decrement on the broad lines (3.4), the flux of the Hβ broad component appears quite weak with respect to the [O III] line. However, the ratio between the luminosity of the broad Hα line and the 2–10 keV luminosity

Table 11. Properties of the two ULX candidates appeared in the new *XMM–Newton* observation of NGC 4698. See the text for details.

Name	RA	Dec.	Γ	F_s	F_h	L
(1)	(2)	(3)	(4)	(5)	(6)	(7)
XMMU J124820.8+082918	12:48:20.8	+08:29:18.4	1.52 ± 0.13	1.91	4.6	1.6
XMMU J124823.1+082802	12:48:23.1	+08:28:02.5	1.56 ± 0.16	1.29	2.9	1.0

Notes. Col. (1) Name of the source following the naming conventions suggested by the *XMM–Newton* team. (2) and (3) RA and Dec. (equatorial J2000). (4) X-ray photon index. (5) and (6) 0.5–2 and 2–10 keV fluxes are in 10^{-14} erg s^{-1} cm^{-2}. (7) 0.5–10 keV luminosities are in 10^{39} erg s^{-1}.

($L_{\rm H\alpha}^{\rm broad}/L_{2-10\,\rm keV} \simeq -1.7$) is still within the distribution presented by Shi et al. (2010) for type 1 and intermediate AGN. Therefore, the BLR in this source may be somewhat weaker than that in 'normal' AGN, but the source cannot be considered a true type 2 Seyfert galaxy.

Other two sources, IRAS 01428−0404 and NGC 4698, are very likely Compton thick. In both cases, the optical classification as a Sy2 is unambiguous. On the other hand, the presence of a Compton-thick absorber cannot be directly confirmed by the X-ray spectral analysis, because of the weakness of the sources. However, the low 2–10 keV to [O III] luminosity ratios are quite suggestive that the primary X-ray continuum is absorbed by a Compton-thick material along the line of sight, while we only observe a small fraction as reflected by circumnuclear matter. If this interpretation is correct, the two sources are standard Compton-thick Sy2 galaxies, and must be cancelled from any list of unabsorbed Sy2 candidates.

5.2 Mrk 273x: a peculiar candidate

One object of our initial sample, Mrk 273x, represents a good candidate as an unabsorbed Sy2. However, the optical classification as a Sy2 is only based on the lack of a broad component of the Hβ emission line: a spectrum encompassing the Hα emission line region is definitely needed to settle the issue. Interestingly enough, its X-ray luminosity is very large ($\simeq 10^{44}$ erg s^{-1}). Adopting different bolometric corrections for the X-ray luminosity (Elvis et al. 1994; Marconi et al. 2004; Vasudevan & Fabian 2009), we obtain bolometric luminosities in the range of $1–3 \times 10^{45}$ erg s^{-1}. Although no BH mass estimates are present in the literature, we can have a rough one by using the FWHM of the [O III] emission line as a proxy of the stellar velocity dispersion (see e.g. Greene & Ho 2005), and then using the Tremaine et al. (2002) relation. With the FWHM reported by Xia et al. (1999), we get a BH mass of $\simeq 1 \times 10^8$ M$_\odot$. Therefore, the Eddington rate of Mrk 273x would be of the order of 0.08–0.2. If this source is confirmed to really lack the BLR, the models invoking a low accretion rate/low luminosity regime for its disappearance would be seriously challenged (see the next section).

This source closely resembles 1ES 1927+654, a luminous type 2 Seyfert galaxy ($L_{0.1-2.4\rm keV} \sim 4.6 \times 10^{43}$ ergs s^{-1}) which revealed persistent, rapid and large-scale variations in *ROSAT* and *Chandra* observations, and no X-ray absorption (Boller et al. 2003). Our campaign of quasi-simultaneous TNG optical/NIR and *XMM–Newton* observations has confirmed the 'true' type 2 nature of this source, i.e. no broad optical emission line components nor X-ray absorption in excess to the Galactic one (Panessa et al., in preparation). However, the *XMM–Newton* flux is 10 times lower than the *ROSAT* one, so the engine might be still strongly active and variable (caught in a low flux state) or may be fading away. The Eddington ratio derived from the *XMM–Newton* flux is $L_{\rm Bol}/L_{\rm Edd} \sim 0.01$, still at the borderline of the critical accretion rates predicted by theoretical models (see the next section).

Table 12. Main properties of the three true type 2 Sy2s confirmed in this paper. See the text for details.

Name	L	$M_{\rm BH}$	$L_{\rm bol}/L_{\rm Edd}$
(1)	(2)	(3)	(4)
NGC 3147	0.3−0.7	20−62	4×10^{-5}−3×10^{-4}
NGC 3660	1−2	0.68−2.1	4×10^{-3}−2×10^{-2}
Q2131−427	20−30	77	$2–3 \times 10^{-3}$

Notes. Col. (1) Name of the source. (2) Bolometric luminosity range in 10^{43} erg s^{-1} (see the text for details on the adopted methods for this estimate). (3) BH mass range in 10^7 M$_\odot$ (see the text for the appropriate references). (4) Eddington ratio range.

5.3 True type 2 Sy2s: NGC 3147, NGC 3660 and Q2131−427

Out of the initial sample composed of eight sources, three, namely NGC 3147, NGC 3660 and Q2131−427, do appear to simultaneously lack the broad optical lines and X-ray absorption along the line of sight (see Table 12).[2] In all cases, although a Compton-thick interpretation of the X-ray spectrum cannot be completely excluded (see Brightman & Nandra 2008; Panessa et al. 2009; Matt et al. 2012), the short-term X-ray variability of NGC 3660, the variability on a time-scale of a few years of NGC 3147 and the large optical brightness variability of Q2131−427 strongly support their unabsorbed nature. In order to rule out the presence of broad optical lines in these sources as for standard unobscured AGN, we should compare the weak broad components compatible with their optical spectra to the expectations for 'normal' objects.

In the case of NGC 3147, Bianchi et al. (2008) reported an upper limit to a broad (FWHM = 2000 km s^{-1}) component of Hα corresponding to a luminosity of 2×10^{38} erg s^{-1}. This value is significantly lower than that expected from the X-ray luminosity, i.e. $\simeq 5.6 \times 10^{40}$ erg s^{-1}, considering the relation presented by Stern & Laor (2012), based on a large sample of SDSS type 1 AGN. Similarly, the observed luminosity of the weak broad component of Hα in NGC 3660 is 6.2×10^{39} erg s^{-1}, again significantly lower than the expected value, $\simeq 2.8 \times 10^{41}$ erg s^{-1}. For Q2131−427, the upper limit (FWHM = 4000 km s^{-1}) is 8×10^{40} erg s^{-1} (Panessa et al. 2009), to be compared to the expected 8×10^{42} erg s^{-1}. The same conclusions can be drawn by comparing the observed $L_{\rm H\alpha}^{\rm broad}/L_{2-10\,\rm keV}$ ratios of NGC 3147, NGC 3660 and Q2131−427 to the distribution presented by Shi et al. (2010) for type 1 and

[2] The optical and X-ray observations of NGC 3660 are not strictly simultaneous due to technical problems, but all the available optical spectra are consistent each other, as described in Section 4.5.

intermediate AGN. In the case of NGC 3147 this is also true for the $L^{\rm broad}_{\rm H\beta}/\nu L_\nu^{1.4\,\rm GHz}$ and $L^{\rm broad}_{\rm H\alpha}/L_\nu^{10\,\mu\rm m}$ ratios (Shi et al. 2010). Therefore, in these sources the emission of the BLR, if present, is much weaker than the one found in common Seyfert 1s, or the widths of the broad optical line components are much larger.

Reverberation mapping studies show that the radius of the BLR and the bolometric luminosity of the AGN always follow a tight $L^{1/2}$ relation (see e.g. Kaspi et al. 2007, who showed how the C IV emission line lags follow this relation over more than seven orders of magnitude in continuum luminosity). This relation is naturally explained by assuming that the outer boundary of the BLR is determined by the dust sublimation radius, which is set by the continuum luminosity. Once the BLR radius is determined by the luminosity, the BH mass sets the velocity of the gas at that distance. In formulae, combining equations 2 and 6 in Stern & Laor (2012), we get the expected FWHM of the broad optical lines as a function of the BH mass and the bolometric luminosity of the AGN:

$$\rm FWHM_{H\alpha} \simeq 7088 \left(\frac{\mathit{M}_{BH}}{10^8\,M_\odot}\right)^{0.49} \left(\frac{\mathit{L}_{bol}}{10^{44}}\right)^{-0.26} km\,s^{-1}. \quad (2)$$

The bolometric luminosity of NGC 3147 can be estimated from the 2–10 keV X-ray luminosity, whose average value around 3×10^{41} erg s^{-1} was measured by *XMM–Newton* (Bianchi et al. 2008) and *Suzaku* (Matt et al. 2012). Adopting different bolometric corrections for the X-ray luminosity (Elvis et al. 1994; Marconi et al. 2004; Vasudevan & Fabian 2009), we obtain bolometric luminosities in the range 3–7 $\times$ 10^{42} erg s^{-1}. On the other hand, BH mass estimates in the literature range from 2.0 to 6.2 $\times$ 10^8 M$_\odot$ (Merloni, Heinz & di Matteo 2003; Dong & De Robertis 2006). Using these estimates in equation (2), the expected FWHM for the Hα emission line produced in the BLR should be in the range 20 000–40 000 km s^{-1}. Objects with such broad lines are expected to be extremely rare, if existing at all (see e.g. Stern & Laor 2012).

In the case of NGC 3660, from the X-ray luminosity measured in Section 4.5 we get bolometric luminosities in the range 1–2 $\times$ 10^{43} erg s^{-1}. With BH mass estimates ranging from 6.8 $\times$ 10^6 (Meléndez, Kraemer & Schmitt 2010) to 2.1 $\times$ 10^7 M$_\odot$ (Wang & Zhang 2007), the expected FWHM for the broad Hα component is 2800–6000 km s^{-1}. This value is consistent with the FWHM of the broad component possibly detected in our optical spectra (but not confirmed in the IR spectrum: see Section 4.5), whose luminosity, as shown above, is significantly lower than the one expected from a 'normal' BLR.

Finally, from the X-ray luminosity of Q2131−427 and the BH mass (7.7 $\times$ 10^8 M$_\odot$) reported by Panessa et al. (2009), we get bolometric luminosities in the range 2–3 $\times$ 10^{44} erg s^{-1}, and an expected FWHM for the broad Hα component of 14 000–16 000 km s^{-1}. These values, even if less extreme than those derived for NGC 3147, are still exceptional.

The weakness of the broad optical lines may be due to dust extinction, as in normal Sy2s. The amount of dust required is very large, since the broad lines are not present even in the NIR spectra (see Section 4.5 for NGC 3660 and Tran et al. 2011, for NGC 3147). However, in the X-ray spectra of these sources there are no signatures of absorption by cold gas along the line of sight, requiring an anomalous high fraction of dust associated with very little gas. Although deviations from the Galactic gas-to-dust ratios are very common in AGN (e.g. Maiolino et al. 2001), there is always more gas than expected, likely explained by the presence of absorbing gas within the dust sublimation radius (e.g. Bianchi et al. 2012, and references therein). The opposite situation, i.e. more dust than standard, would imply the presence of an unlikely physical mechanism able to suppress gas without destroying dust. In principle a very highly ionized dusty warm absorber could be difficult to detect in these X-ray spectra without high spectral resolution and high statistics. However, the properties of such a dusty warm absorber should be much more extreme than those typically found in Seyfert 1 galaxies (e.g. Lee et al. 2001, and references therein). Alternatively, an ad hoc geometry could account for dust extinction of the BLR, but no gas absorption along the line of sight to the X-ray source. However, this peculiar geometry should also prevent us from seeing the optical broad lines even in polarized light: both sources have high-quality spectropolarimetric data, with no evidence for a hidden BLR (Tran 2003; Shi et al. 2010; Tran et al. 2011).

The most likely explanation for the absence of broad optical lines in these sources is that they intrinsically lack the BLR. The inability of some AGN to form the BLR is predicted by several theoretical models, all based on a rich literature elaborating the idea that the BLR is part of a disc wind (e.g. Emmering, Blandford & Shlosman 1992; Murray et al. 1995; Elvis 2000). Evidence in favour of the presence of this wind in Seyfert galaxies is likely represented by the observation of X-ray and UV absorbers outflowing up to very high velocities (e.g. Blustin et al. 2005; Tombesi et al. 2010). Nicastro (2000) and Trump et al. (2011) assume that this disc wind originates at the radius where radiation pressure is equal to the gas pressure. If this radius becomes smaller than a characteristic critical radius, then the disc wind cannot be launched, and the BLR cannot from. This critical radius can be identified with the innermost last stable orbit of a classic Shakura & Sunyaev (1973) disc (Nicastro 2000), or the transition radius to a radiatively inefficient accretion flow (Trump et al. 2011). In both cases, the formation of the BLR is prevented for Eddington rates $\dot{m} = L_{\rm bol}/L_{\rm Edd}$ lower than a critical value, which can be expressed as $\dot{m} \simeq 2.4 \times 10^{-3}\,M_8^{-1/8}$ and $1.3 \times 10^{-2}\,M_8^{-1/8}$, respectively, where M_8 is the BH mass in units of 10^8 M$_\odot$. The Eddington rate of NGC 3147, with the same considerations as above, can be estimated in the range 4×10^{-5}–3×10^{-4}, well below the thresholds predicted by both models. The same holds for Q2131−427, where $\dot{m} = 2$–3×10^{-3}. In the case of NGC 3660, $\dot{m} = 4 \times 10^{-3}$–$2 \times 10^{-2}$, lower than the Trump et al. (2011) threshold, but only marginally consistent with the Nicastro (2000) one in the low end.

Trump et al. (2011) support their model by showing an observational limit at $\dot{m} \simeq 0.01$ between AGN with broad optical lines and (X-ray unobscured) AGN without broad optical lines. Another observational evidence of the existence of a minimum accretion rate for the formation of the BLR comes from several studies that point out the absence of broad optical lines in the spectra in polarized light of Sy2s with low Eddington rates (e.g. Nicastro et al. 2003; Bian & Gu 2007; Wu et al. 2011; Marinucci et al. 2012). In the recent analysis by Marinucci et al. (2012), the threshold was found at $\dot{m} \simeq 0.01$, which is in agreement both with the model and the data presented by Trump et al. (2011).

Are true type Sy2s rare objects? Apart from NGC 3147, NGC 3660 and Q2131−427, there are not many other strong representatives of this class in the literature. If all true type Sy2s are indeed low accretors, their paucity should not be very surprising. As already noted by Marinucci et al. (2012) and Bianchi et al. (2012), when a sizeable sample of X-ray unobscured radio-quiet AGN with good-quality spectra is analysed (e.g. CAIXA; Bianchi et al. 2009a), only a few (<5 per cent) lie below the $\dot{m} \simeq 0.01$ limit, with NGC 3147 and NGC 3660 among them. The fraction of low-accreting unabsorbed Sy2 candidates rises up to 30 per cent in extensively studied samples derived from surveys (COSMOS; Trump et al. 2011), but the lack of simultaneous optical and X-ray observations, and the

low quality of the X-ray spectra, prevent us from drawing firm conclusions on their nature as genuine true type 2 AGN. Interestingly, a similar fraction of $\simeq$25 per cent of low-accreting objects are found to lack the signatures of a hidden BLR in polarized light in obscured AGN (Marinucci et al. 2012). In this scenario, these sources would represent the obscured counterparts of true type Sy2s, the only difference being the presence of an obscuring medium along the line of sight.

A separate discussion is probably needed for the so-called low-luminosity AGN (LLAGN), which are mostly LINERs or transition objects, with bolometric luminosities significantly lower than 10^{42} erg s^{-1} (e.g. Ho et al. 1997b; Terashima, Ho & Ptak 2000). There are some LLAGN accreting at rates well below 0.01 with broad optical emission lines (e.g. M81; Ho, Filippenko & Sargent 1996). Recently, Elitzur & Ho (2009) presented a comprehensive analysis of a sample of LLAGN with the aim to derive observationally where the separation between objects with BLR and those without lies. The separation they propose can be expressed in terms of accretion rate as $\dot{m} \simeq 1.8 \times 10^{-6}\, M_8^{-1/3}$, much lower than the ones predicted by the Trump et al. (2011) and Nicastro (2000) models (with which our results agree), despite adopting a similar disc-wind scenario. Trump et al. (2011) discussed in detail this discrepancy, without reaching a definite conclusion. It seems that the formation of the BLR in objects with very inefficient accretion regimes may be significantly different than what occurs in higher luminosity AGN. Further studies on LLAGN are clearly fundamental to understand this issue and to shed light on the link between the accretion mechanisms and the formation of the BLR.

ACKNOWLEDGMENTS

We thank A. Laor and J. Stern for useful discussions, and the anonymous referee for helping us in improving the manuscript. SB, GM and AW acknowledge financial support from ASI (grant 1/023/05/0). FP acknowledges support from *INTEGRAL* ASI I/033/10/0, and FP and AW from ASI/INAF I/009/10/0. XB and FJC acknowledge partial financial support from the Spanish Ministerio de Ciencia e Innovación project AYA2010-21490-C02-01.

REFERENCES

Antonucci R., 1993, ARA&A, 31, 473
Arnaud K. A., 1996, in Jacoby G. H., Barnes J., eds, ASP Conf. Ser. Vol. 101, Astronomical Data Analysis Software and Systems V. Astron. Soc. Pac., San Francisco, p. 17
Awaki H., Koyama K., 1993, Adv. Space Res., 13, 221
Balestra I., Boller T., Gallo L., Lutz D., Hess S., 2005, A&A, 442, 469
Barvainis R., 1987, ApJ, 320, 537
Bentz M. C., Peterson B. M., Netzer H., Pogge R. W., Vestergaard M., 2009, ApJ, 697, 160
Bian W., Gu Q., 2007, ApJ, 657, 159
Bianchi S., Guainazzi M., Chiaberge M., 2006, A&A, 448, 499
Bianchi S., Corral A., Panessa F., Barcons X., Matt G., Bassani L., Carrera F. J., Jiménez-Bailón E., 2008, MNRAS, 385, 195
Bianchi S., Guainazzi M., Matt G., Fonseca Bonilla N., Ponti G., 2009a, A&A, 495, 421
Bianchi S., Piconcelli E., Chiaberge M., Bailón E. J., Matt G., Fiore F., 2009b, ApJ, 695, 781
Bianchi S., Maiolino R., Risaliti G., 2012, Adv. Astron, 2012, id. 782030
Blustin A. J., Page M. J., Fuerst S. V., Branduardi-Raymont G., Ashton C. E., 2005, A&A, 431, 111
Boller T., Meurs E. J. A., Brinkmann W., Fink H., Zimmermann U., Adorf H.-M., 1992, A&A, 261, 57
Boller T., Bertoldi F., Dennefeld M., Voges W., 1998, A&AS, 129, 87
Boller T. et al., 2003, A&A, 397, 557
Bowen I. S., 1960, ApJ, 132, 1
Brightman M., Nandra K., 2008, MNRAS, 390, 1241
Cappi M. et al., 2006, A&A, 446, 459
Cash W., 1976, A&A, 52, 307
Cid Fernandes R., Gu Q., Melnick J., Terlevich E., Terlevich R., Kunth D., Rodrigues Lacerda R., Joguet B., 2004, MNRAS, 355, 273
Contini T., Considere S., Davoust E., 1998, A&AS, 130, 285
Corral A., Barcons X., Carrera F. J., Ceballos M. T., Mateos S., 2005, A&A, 431, 97
Corsini E. M., Méndez-Abreu J., Pastorello N., Dalla Bontà E., Morelli L., Beifiori A., Pizzella A., Bertola F., 2012, MNRAS, 423, L79
Cortese L., Hughes T. M., 2009, MNRAS, 400, 1225
Cusumano G. et al., 2010, A&A, 524, A64
Dadina M., 2007, A&A, 461, 1209
della Ceca R., Braito V., Cagnoni I., Maccacaro T., 2001, Mem. Soc. Astron. Ital., 72, 841
Dong X. Y., De Robertis M. M., 2006, AJ, 131, 1236
Elitzur M., Ho L. C., 2009, ApJ, 701, L91
Elvis M., 2000, ApJ, 545, 63
Elvis M. et al., 1994, ApJS, 95, 1
Elvis M., Risaliti G., Nicastro F., Miller J. M., Fiore F., Puccetti S., 2004, ApJ, 615, L25
Emmering R. T., Blandford R. D., Shlosman I., 1992, ApJ, 385, 460
Fabbiano G., Kim D.-W., Trinchieri G., 1992, ApJS, 80, 531
Georgantopoulos I., Zezas A., 2003, ApJ, 594, 704
Georgantopoulos I., Papadakis I., Zezas A., Ward M. J., 2004, ApJ, 614, 634
Gilli R., Maiolino R., Marconi A., Risaliti G., Dadina M., Weaver K. A., Colbert E. J. M., 2000, A&A, 355, 485
Gliozzi M., Sambruna R. M., Foschini L., 2007, ApJ, 662, 878
Gliozzi M. et al., 2010, ApJ, 725, 2071
Gonçalves A. C., Véron-Cetty M.-P., Véron P., 1999, A&AS, 135, 437
González-Martín O., Masegosa J., Márquez I., Guainazzi M., Jiménez-Bailón E., 2009, A&A, 506, 1107
Greene J. E., Ho L. C., 2005, ApJ, 627, 721
Gu Q., Melnick J., Cid Fernandes R., Kunth D., Terlevich E., Terlevich R., 2006, MNRAS, 366, 480
Guainazzi M., Fabian A. C., Iwasawa K., Matt G., Fiore F., 2005a, MNRAS, 356, 295
Guainazzi M., Matt G., Perola G. C., 2005b, A&A, 444, 119
Hawkins M. R. S., 2004, A&A, 424, 519
Ho L. C., Filippenko A. V., Sargent W. L. W., 1996, ApJ, 462, 183
Ho L. C., Filippenko A. V., Sargent W. L. W., 1997a, ApJS, 112, 315
Ho L. C., Filippenko A. V., Sargent W. L. W., Peng C. Y., 1997b, ApJS, 112, 391
Imanishi M., 2003, ApJ, 599, 918
Immler S., Lewin W. H. G., 2003, in Weiler K., ed., Lecture Notes in Physics, Vol. 598, Supernovae and Gamma-ray Bursters. Springer-Verlag, Berlin, p. 91
Iwasawa K., 1999, MNRAS, 302, 96
Kaspi S., Brandt W. N., Maoz D., Netzer H., Schneider D. P., Shemmer O., 2007, ApJ, 659, 997
Kewley L. J., Groves B., Kauffmann G., Heckman T., 2006, MNRAS, 372, 961
Kirhakos S. D., Steiner J. E., 1990, AJ, 99, 1722
Kollatschny W., Biermann P., Fricke K. J., Huchtmeier W., Witzel A., 1983, A&A, 119, 80
Lamastra A., Bianchi S., Matt G., Perola G. C., Barcons X., Carrera F. J., 2009, A&A, 504, 73
Lee J. C., Ogle P. M., Canizares C. R., Marshall H. L., Schulz N. S., Morales R., Fabian A. C., Iwasawa K., 2001, ApJ, 554, L13
Maiolino R., Marconi A., Salvati M., Risaliti G., Severgnini P., Oliva E., La Franca F., Vanzi L., 2001, A&A, 365, 28
Marconi A., Risaliti G., Gilli R., Hunt L. K., Maiolino R., Salvati M., 2004, MNRAS, 351, 169
Marinucci A., Bianchi S., Nicastro F., Matt G., Goulding A. D., 2012, ApJ, 748, 130

Matt G., Bianchi S., Guainazzi M., Barcons X., Panessa F., 2012, A&A, 540, A111
Meléndez M., Kraemer S. B., Schmitt H. R., 2010, MNRAS, 406, 493
Merloni A., Heinz S., di Matteo T., 2003, MNRAS, 345, 1057
Moran E. C., Halpern J. P., Helfand D. J., 1996, ApJS, 106, 341
Murray N., Chiang J., Grossman S. A., Voit G. M., 1995, ApJ, 451, 498
Nicastro F., 2000, ApJ, 530, L65
Nicastro F., Martocchia A., Matt G., 2003, ApJ, 589, L13
Panessa F., Bassani L., 2002, A&A, 394, 435
Panessa F., Bassani L., Cappi M., Dadina M., Barcons X., Carrera F. J., Ho L. C., Iwasawa K., 2006, A&A, 455, 173
Panessa F. et al., 2009, MNRAS, 398, 1951
Pappa A., Georgantopoulos I., Stewart G. C., Zezas A. L., 2001, MNRAS, 326, 995
Persic M., Rephaeli Y., 2002, A&A, 382, 843
Piconcelli E., Jimenez-Bailón E., Guainazzi M., Schartel N., Rodríguez-Pascual P. M., Santos-Lleó M., 2004, MNRAS, 351, 161
Pietsch W., Bischoff K., Boller T., Doebereiner S., Kollatschny W., Zimmermann H.-U., 1998, A&A, 333, 48
Puccetti S., Fiore F., Risaliti G., Capalbi M., Elvis M., Nicastro F., 2007, MNRAS, 377, 607
Ranalli P., Comastri A., Setti G., 2003, A&A, 399, 39
Risaliti G., Gilli R., Maiolino R., Salvati M., 2000, A&A, 357, 13
Risaliti G., Elvis M., Fabbiano G., Baldi A., Zezas A., 2005, ApJ, 623, L93
Risaliti G., Nardini E., Salvati M., Elvis M., Fabbiano G., Maiolino R., Pietrini P., Torricelli-Ciamponi G., 2011, MNRAS, 410, 1027
Ruiz A., Miniutti G., Panessa F., Carrera F. J., 2010, A&A, 515, A99
Sargsyan L. A., Weedman D. W., 2009, ApJ, 701, 1398
Sekiguchi K., Wolstencroft R. D., 1993, MNRAS, 263, 349
Shakura N. I., Sunyaev R. A., 1973, A&A, 24, 337
Shi Y., Rieke G. H., Smith P., Rigby J., Hines D., Donley J., Schmidt G., Diamond-Stanic A. M., 2010, ApJ, 714, 115
Shu X. W., Wang J. X., Jiang P., Fan L. L., Wang T. G., 2007, ApJ, 657, 167
Shu X. W., Liu T., Wang J. X., 2010, ApJ, 722, 96
Stern J., Laor A., 2012, preprint (arXiv:e-prints)
Teng S. H. et al., 2009, ApJ, 691, 261
Terashima Y., Wilson A. S., 2003, ApJ, 583, 145
Terashima Y., Ho L. C., Ptak A. F., 2000, ApJ, 539, 161
Tombesi F., Cappi M., Reeves J. N., Palumbo G. G. C., Yaqoob T., Braito V., Dadina M., 2010, A&A, 521, A57
Tran H. D., 2001, ApJ, 554, L19
Tran H. D., 2003, ApJ, 583, 632
Tran H. D., Lyke J. E., Mader J. A., 2011, ApJ, 726, L21
Tremaine S. et al., 2002, ApJ, 574, 740
Trump J. R. et al., 2011, ApJ, 733, 60
Vasudevan R. V., Fabian A. C., 2009, MNRAS, 392, 1124
Wang J.-M., Zhang E.-P., 2007, ApJ, 660, 1072
Wolter A., Gioia I. M., Henry J. P., Mullis C. R., 2005, A&A, 444, 165
Wu Y.-Z., Zhang E.-P., Liang Y.-C., Zhang C.-M., Zhao Y.-H., 2011, ApJ, 730, 121
Xia X.-Y., Mao S., Wu H., Liu X.-W., Gao Y., Deng Z.-G., Zou Z.-L., 1999, ApJ, 524, 746
Xia X. Y., Xue S. J., Mao S., Boller T., Deng Z. G., Wu H., 2002, ApJ, 564, 196

This paper has been typeset from a TEX/LATEX file prepared by the author.